Localizing Carbohydrate Binding Sites in Proteins using Hydrogen/Deuterium Exchange Mass Spectrometry

Jingjing Zhang[1], Elena N. Kitova[1], Jun Li[1], Luiz Eugenio[2], Kenneth Ng[2] and John S. Klassen[1]*

Alberta Glycomics Centre and

[1]Department of Chemistry, University of Alberta, Edmonton, Alberta, Canada T6G 2G2

[2]Department of Biological Sciences, University of Calgary, Calgary, Alberta, Canada T2N 1N4

Abstract

The application of hydrogen/deuterium exchange mass spectrometry (HDX-MS) to localize ligand binding sites in carbohydrate-binding proteins is described. Proteins from three bacterial toxins, the B subunit homopentamers of Cholera toxin and Shiga toxin type 1 and a fragment of *Clostridium difficile* toxin A, and their interactions with native carbohydrate receptors, GM_1 pentasaccharide (β-Gal-(1→3)-β-GalNAc-(1→4)[α-Neu5Ac-(2→3)]-β-Gal-(1→4)-Glc), Pk trisaccharide (α-Gal-(1→4)-β-Gal-(1→4)-Glc) and CD-grease (α-Gal-(1→3)-β-Gal-(1→4)-β-GlcNAcO$(CH_2)_8CO_2CH_3$), respectively, served as model systems for this study. Comparison of the differences in deuterium uptake for peptic peptides produced in the absence and presence of ligand revealed regions of the proteins that are protected against deuterium exchange upon ligand binding. Notably, protected regions generally coincide with the carbohydrate binding sites identified by X-ray crystallography. However, ligand binding can also result in increased deuterium exchange in other parts of the protein, presumably through allosteric effects. Overall, the results of this study suggest that HDX-MS can serve as a useful tool for localizing the ligand binding sites in carbohydrate-binding proteins. However, a detailed interpretation of the changes in deuterium exchange upon ligand binding can be challenging due to the presence of ligand-induced changes in protein structure and dynamics.

Introduction

Protein-carbohydrate interactions are implicated in a wide range of cellular processes, including cell-cell and cell-matrix interactions, signal transduction, inflammation, cancer metastasis, bacterial and viral infections and the immune response [1]. Elucidating the structures of protein-carbohydrate complexes, as well as the kinetics and thermodynamics of the interactions, is vital to a complete understanding of many physiological and pathological cellular processes and can guide drug discovery and design efforts [2-4]. High resolution techniques, such as X-ray crystallography and nuclear magnetic resonance spectroscopy, have been extensively used to elucidate the three dimensional structures of protein-carbohydrate complexes [5-7]. However, many such interactions are not amenable to these techniques due to limitations associated with protein size, solubility or ease of crystallization, as well as the cost and availability of pure oligosaccharide ligands [8]. Consequently, there is a need for alternative structural techniques capable of probing protein-carbohydrate interactions.

Recently, hydrogen/deuterium exchange mass spectrometry (HDX-MS) has emerged as a promising method for characterizing the interactions between proteins and their ligands [9-13]. When a ligand binds to a protein some of the amide H's may become (more) protected against exchange (due to the formation of new or stronger inter- or intramolecular H-bonds or a reduction in solvent accessibility), resulting in decreased rates of exchange for the peptides containing these groups [10,17]. Consequently, comparison of the D-uptake for peptides produced from the ligand-bound and unbound forms of a protein can, in principle, reveal residues involved in ligand binding [18]. HDX-MS has been applied to a variety of non-covalent protein complexes, including protein-protein and multiprotein complexes [16,19], antibody-

antigen [20], protein-peptide [21], and protein-small molecule complex [22,23]. Additionally, it has been used to study ligand-induced changes in protein conformation and dynamics [18,24-26].

To date, however, there have been few HDX-MS studies reported for protein-carbohydrate interactions [27-29]. One possible reason for this is the low affinities that are typical of protein-carbohydrate interactions (association constants (K_a) of ~10^3 M^{-1} [3]). In order to obtain detectable differences in peptide D-uptake, high ligand occupancy (approaching saturation of the binding site) is needed. A large and sometimes prohibitive amount of carbohydrate ligand is required to achieve this condition in the case of low affinity interactions. Another consideration is the relatively small size of many carbohydrate ligands, typically mono-, di- or tri-saccharide. Binding of small ligands, which form few intermolecular interactions, generally affords protection to only a few residues in the protein. Moreover, binding is usually dominated by intermolecular interactions involving amino acid side chains, rather than the peptide backbone, which may offer limited protection to the amide H's. Finally, carbohydrate binding can be accompanied by changes in protein structure and dynamics. These changes may lead to a decrease or increase in D-uptake of residues remote from the carbohydrate binding site [29,30]. Consequently, the measured differences in peptide D-uptake may reflect the formation of intermolecular interactions or ligand binding-induced changes in protein conformation or dynamics, or a combination of these effects [9,10]. Additionally, ligand-induced changes in the population of different protein conformers may also affect the rate of D-uptake [17, 31, 32]. It has been proposed that docking simulations or site-directed mutagenesis, in combination with HDX-MS data may help to localize the ligand binding site [18,30]. Alternative strategies to distinguish direct ligand protection from ligand-induced changes in protein dynamics or conformation involve comparing the HDX-MS profiles measured for the protein binding to a

homologous series of ligands [33] or through the use of a second ligand, which binds at an alternative site and suppresses allosteric effects [34].

Here, HDX-MS was applied to proteins from three bacterial toxins, the B subunit homopentamers of Cholera toxin (CTB_5) and Shiga toxin 1 ($Stx1B_5$) and a fragment of *Clostridium difficile* toxin A (TcdA-A2), and their interactions with native carbohydrate receptors, GM_1 pentasaccharide (GM_1-os, β-Gal-(1→3)-β-GalNAc-(1→4)[α-Neu5Ac-(2→3)]-β-Gal-(1→4)-Glc), Pk trisaccharide (Pk-OH, α-Gal-(1→4)-β-Gal-(1→4)-Glc), which is the oligosaccharide of the globotrioside Gb3, and CD-grease (α-Gal-(1→3)-β-Gal-(1→4)-β-$GlcNAcO(CH_2)_8CO_2CH_3$), respectively, to test the reliability of the method for localizing carbohydrate binding sites. Crystal structures have been reported for all three protein-carbohydrate complexes (Figure 1). It is known that CTB_5 has five GM_1-os binding sites and the step-wise association constants range from 10^6 to 10^7 M^{-1} [35]. According to the crystal structure reported for the (CTB_5 + 5GM_1-os) complex (PDB 3CHB), each GM_1-os interacts primarily with a single subunit, with the binding site formed by three loops (loop 1- loop 3) from the same subunit and a fourth loop (loop 4) containing residues from the adjacent subunit (Figure 1a) [35]. Although it is known that the stepwise binding of GM_1-os to CTB_5 exhibits positive cooperativity [34], no obvious protein conformational change is detectable (based on X-ray crystallography) upon ligand binding [35]. $Stx1B_5$ is structurally similar to CTB_5. According to the reported crystal structure (PDB 1BOS), each subunit of $Stx1B_5$ can bind up to three Pk trisaccharide ligands (Figure 1b). The three binding sites (referred to as *site 1*, *site 2* and *site 3*) are located on the same face of the homopentamer [36]. *Site 1* is composed of residues within a single subunit, while *site 2* and *site 3* also contain residues from adjacent subunits. According to available binding data, the three binding sites are independent and non-equivalent, with Pk

binding preferentially to *site 2*, although with low affinity, ~350 M^{-1} [37,38]. Based on crystallographic data available for free (PDB 2XSC) and Pk-bound $Stx1B_5$, no significant conformational change occurs upon Pk binding [39]. The TcdA-A2 fragment is from the C-terminal repetitive domain of TcdA, which contains nine short repeats separated by two long repeats [40]. Within the TcdA-A2 fragment, a long repeat and the following short repeat create a shallow carbohydrate binding site, and two carbohydrate binding sites are present in the fragment (PDB 2G7C) [40]. Previous studies showed that TcdA-A2 displays a low affinity for CD-grease, with an apparent K_a of ~500 M^{-1} at 25 °C, and that the two binding sites exhibit similar affinities [41].

Experimental Methods

Materials

CTB_5 (MW 58,020 Da) was purchased from Sigma-Aldrich Canada (Oakville, ON, Canada). A stock solution (60 µM) of CTB_5 was prepared by dissolving a known amount of protein in ultrafiltered water (Milli-Q; Millipore, Billerica, MA, USA) and was stored at 4 °C until needed. $Stx1B_5$ (MW 38,450 Da) was a gift from Prof. G. Armstrong (Univ. of Calgary) as a stock solution prepared in 0.05 M Tris buffer (pH 7.5). TcdA-A2 (MW 29,575 Da) was expressed and purified as previously described [40]. The TcdA-A2 stock solution was at a concentration of 57.5 µM in 60 mM imidazole (pH 7.0), 150 mM NaCl and 50 g L^{-1} glycerol (>99.5% purity). Both $Stx1B_5$ and TcdA-A2 stock solutions were stored at -80 °C until needed. Prior to analysis, the protein solutions were diluted with Milli-Q water to the desired concentrations. GM_1-os (β-Gal-(1→3)-β-GalNAc-(1→4)[α-Neu5Ac-(2→3)]-β-Gal-(1→4)-Glc, MW 998.9 Da), and Pk-OH (α-Gal-(1→4)-β-Gal-(1→4)-Glc, MW 504.4 Da) were purchased from Elicityl SA (Crolles, France). CD-grease (α-Gal-(1→3)-β-Gal-(1→4)-β-GlcNAcO$(CH_2)_8CO_2CH_3$, MW 715.7 Da)

was a gift form Prof. D. Bundle (Univ. of Alberta). Stock solutions of each of the carbohydrate ligands were prepared by dissolving a known amount of solid in Milli-Q water to give a final concentration of 1 mM (GM_1-os) or 0.4 M (Pk-OH and CD-grease); the stock solutions were stored at -20 °C until needed.

HDX-MS

The HDX-MS experiments were carried out using a Synapt G2-S HDMS mass spectrometer equipped with a nanoACQUITY UPLC system with HDX technology (Waters, UK), and a PAL HTX-*xt* automatic sample preparation and injection system. Two sample stacks in the PAL system provided accurate temperature control for the labeling reactions (20 °C), and for the reaction quench (1 °C), respectively. Protein solutions (4 µM, 6 µM and 12 µM for CTB_5, $Stx1B_5$ and TcdA-A2, respectively) alone or in the presence of excess ligand (0.2 mM GM_1-os, 0.2 M Pk-OH and 0.2 M CD-grease) were diluted 15-fold with either equilibrium buffer (10 mM potassium phosphate in H_2O at pH 7.0) for control experiments, or labeling buffer (10 mM potassium phosphate in D_2O at pD 7.0) [42] for labeling experiments. Under these experimental conditions, >97% of CTB_5 ligand binding sites are expected to be occupied (assuming a stepwise association constant of 1 x 10^6 M^{-1}, while for $Stx1B_5$ and TcdA-A2 the binding sites are predicted to be 82% and 79% occupied (based on association constants of 350 M^{-1} and 250 M^{-1}, respectively). For the labeling experiments, diluted samples were incubated at 20 °C for time intervals of 1, 5 and 10 min. After that, samples (both for control and labeling experiments) were quenched with quench buffer (4 M guanidine hydrochloride and 0.5 M *tris*(2-carboxyethyl)phosphine (TCEP) in H_2O at pH 2.6 for CTB_5 and $Stx1B_5$, and 4 M guanidine hydrochloride in 100 mM potassium phosphate in H_2O at pH 2.6 for TcdA-A2) using a 1:1 dilution ratio at 1 °C. Quenched samples were incubated for 30 s prior to injection into a 50 µL

injection loop of a nanoACQUITY UPLC system with HDX technology. Online digestion was performed using an immobilized pepsin column (Life Technologies, Burlington, Canada) with 0.1% formic acid in H_2O at a flow rate of 200 µL min^{-1} at 20 °C. Peptic peptides were trapped online using an ACQUITY UPLC BEH C18 1.7 µm VanGuard Pre-column at 1 °C and desalted for 2 min. Peptide separation was carried using an ACQUITY UPLC C18 1.7 µm 1.0×100mm column with a 12 min gradient elution at a flow rate of 40 µL min^{-1}. The content of solvent A (solvent A, 0.1% formic acid and 5% acetonitrile in H_2O; solvent B, 0.1% formic acid in acetonitrile) in the mobile phase was decreased over a 7 min period form 95% to 63% and held constant for 1 min before a further reduction from 63% to 16% over a 0.5 min period. After 0.5 min at 16%, the percentage of solvent A was increased to 95% over a 0.5 min period. The eluent was introduced to the Synapt G2-S HDMS using the ESI source. Mass spectra were acquired in MS^E mode from m/z 50 to 2000 with a scan rate of 0.4 s $scan^{-1}$ and lock-mass correction (using [Glu]-Fibrinopeptide). The capillary and cone voltages were kept constant at 3 kV and 40 V, respectively. At a given labeling time (*t*), the free and ligand-bound protein samples were analyzed back-to-back, with a blank sample (water) in between, to avoid the effects of sample carry-over.

Data analysis

ProteinLynx Global Server 2.5.2 software (PLGS, Waters) was used to identify peptic peptides produced for each protein, in the absence and presence of the ligand, prior to HDX (*i.e.*, at $t = 0$ min). To minimize redundancy, the DynamX 2.0 software (Waters) was used to generate a smaller peptide list consisting of peptides that were detected in all replicate measurements and that provided maximum sequence coverage. The average MW for each peptide was calculated by DynamX using the centroid of the entire envelope of the corresponding isotopic peaks; for each

peptide one or more than one charge states were considered. The D-uptake value (D_i, units of Da) for peptide *i* was determined as the difference of the MW measured for this peptide in labeled and control (no exchange) samples, for all labeling times. Illustrative mass spectra for the peptides considered in this study at deuterium exposure times of 0, 1, 5 and 10 min are shown in Figures S1 – S33, Supplementary Data. The corresponding D-uptake values are shown in Figures S34 – S36, Supplementary Data. The relative D-uptake (ΔD_i, units of Da) was calculated as the difference in the D_i values for peptide *i* measured in the absence and presence of ligand. Back exchange was determined [43] using the model peptide [Glu]-Fibrinopeptide and found to be ~30%. Because the extent of back exchange (during protein digestion and LC separation [14, 44]) was expected to be the same for identical peptides produced in the absence and presence of ligand (under identical experimental conditions), no correction for back exchange was performed [43]. However, given the possibility of differential back exchange [45], no attempt was made to improve the spatial resolution of the exchange data through the subtraction of the ΔD_i values for overlapping peptides. To compare the HDX rates for peptides produced in the absence and presence of ligand the ΔD_i values were summed over all labeling times [13]. Error analysis was carried out using a procedure described previously - the standard deviation in D-uptake values measured in triplicate at different deuterium exposure times was calculated and the corresponding confidence intervals were evaluated at 95% confidence level [13, 46]. Absolute errors in the ΔD_i values were calculated using random error propagation of six errors (three deuterium exposure times for the free and ligand-bound protein) as the square root of the sum of the squares of the absolute errors of D-uptake at three different deuterium exposure times for the free and ligand-bound protein. The ΔD_i values were considered significant if the values exceeded three times the standard deviation. In addition, statistical analysis of the difference in D-uptake

between free and ligand-bound proteins was done using the Student's paired two-tailed *t*-test [47, 48]. The results of the statistical analysis are shown in Tables S1 – S3, Supplementary data.

Results and Discussion

Time-resolved HDX-MS measurements were performed on the free and ligand-bound forms of CTB_5, $Stx1B_5$ and TcdA-A2. A summary of the results obtained for each protein-carbohydrate interaction is given below.

CTB_5 and its interaction with GM_1-os

Pepsin digestion of CTB_5 under denaturing conditions produced approximately eighty different peptides per analysis, of which forty were identified in all measurements. In order to decrease redundancy (while maintaining a high sequence coverage), ΔD_i values of only fourteen of these reproducible peptides, covering 96.1% of CTB monomer sequence, were considered (Figure 2a). It can be seen that, in the presence of GM_1-os, seven of the peptides (4-15, 27-38, 41-55, 49-66, 57-72, 83-94 and 80-103) exhibited a significant decrease in D_i values (leading to positive ΔD_i values ranging from 1.1 to 4.6 Da). It should be noted that peptides 80-103 and 99-103, which share common C-termini, have different retention times (5.4 min and 4.4 min, respectively). This result confirms that peptide 99-103 is an authentic peptic peptide and not a y-ion fragment originating in the gas phase from the dissociation of peptide 80-103. In Figure 2b, the corresponding ΔD_i values are mapped onto the structure of the (CTB_5 + 5GM_1-os) complex for one subunit, with the peptides exhibiting positive ΔD_i values highlighted in red. Notably, the peptides with positive ΔD_i values are from the four loops that make up the binding site for GM_1-os [49,50]. According to the crystal structure, GM_1-os forms direct intermolecular H-bonds with seven residues located within loops 1-3, namely residues E11, H13, E51, Q56, Q61, N90 and K91 (Table 1). With the exception of H13, all of these residues interact with the ligand through

their side chains or backbone carbonyl oxygens, rather than amide H's. Importantly, the present results indicate that the protein-carbohydrate interactions involving amino acid side chains can slow down the exchange rate of the associated backbone amide H's of the peptides containing that residue. The protection may originate from reduced solvent accessibility or changes in the local dynamics of the protein. According to the reported crystal structure, there exists a solvent-mediated H-bond between GM_1-os and the backbone amide H of residue G33 from the adjacent subunit. It is interesting to note that peptide 27-38 exhibited a positive ΔD_i (Figure 2b), suggesting that solvent mediated H-bonds involving amide H's can also influence the rate of exchange [51, 52].

$Stx1B_5$ and its interaction with Pk-OH

Pepsin digestion of $Stx1B_5$ produced approximately seventy different peptides, of which thirty-four were identified in every analysis. Since the Stx1B subunit is a small protein, consisting of only 69 residues, there was significant overlap amongst the proteolytic peptides and the D-uptake of only seven of these, which provided 95.6% sequence coverage, was considered. The corresponding ΔD_i values measured for these seven peptides are shown in Figure 3a. Upon binding of Pk-OH, peptides 1-20, 12-20, 30-40, and 52-66 exhibited modest protection, with ΔD_i values ranging from 0.6 Da to 0.7 Da. Based on the measured retention times for the overlapping peptides 1-20 and 12-20 (5.6 min and 5.0 min, respectively), it was established that peptide12-20 is a peptic peptide. For peptides 40-48, 65-69, the ΔD_i values were smaller (0.2 and 0.3 Da, respectively), indicating little change in protection upon ligand binding. In Figure 3b, the peptides with significant ΔD_i values are highlighted in red for one B subunit in the ($Stx1B_5$ + 15Pk) complex. As noted above, each Stx1B subunit has three Pk binding sites located on one the face of the homopentamer [37]. The residues that make up the binding sites are present in

either a single subunit (*site 1*) or two adjacent subunits (*sites 2* and *3*). Consistent with the reported crystal structure, the HDX-MS results reveal that the peptides exhibiting the greatest protection against exchange upon ligand binding are located within the ligand binding sites, and contain residues involved in direct H-bonds (through side chains or amide groups) with the ligand (Table 1). Because three of the peptides exhibiting increased protection (namely 12-20, 30-40 and 52-66) include amino acid residues that belong to all three sites (*site 1*: D17 and G60, *site 2*: D16, N32, R33, N55 and F63 and *site 3*: D18, W34 and N35), it is not possible to establish the contribution of ligand binding at each of these sites. However, it is notable that for peptide 20-31, which contains residues T21 and E28 and form direct H-bonds with Pk in *site 1*, no protection was observed upon ligand binding. The absence of protection at T21 (the second residue the 20-31 peptide) is likely due to rapid back-exchange. However, examination of the crystal structure reveals that E28 (and T21) is located in a β-sheet and interact with the Pk ligand through the side chain. Therefore, the absence of protection could reflect the fact that the E28 amide H is located in structured regions and, therefore, already experiences a certain degree of protection against exchange. Consequently, the influence of ligand binding on the rate of exchange may not be pronounced, such that no significant difference in D-uptake is observed. In addition, it is also possible that the absence of protection for this peptide reflects the fact that no ligand binding occurs at this site. It has been suggested, based on solution NMR data [53], that the Pk trisaccharide ligand only binds to *site 2*. Since residues T21 and E28 belong to *site 1* (Table 1), the absence of protection can be explained by an absence of binding or, at least, very low ligand occupancy of this binding site at the ligand concentration used.

TcdA-A2 and its interaction with CD-grease

Pepsin digestion of TcdA-A2 produced approximately one hundred different peptides, fifty-four of which were identified in every analysis carried out. The D-uptake values for twenty-three of these peptides, covering 92.4% of the TcdA-A2 sequence, were considered. The ΔD_i values measured for these peptides are shown in Figure 4a and in Table S3, Supplementary data. Notably, the ΔD_i values are small and have significant uncertainties. However, from the results of the statistical analysis (*t*-test), it was possible to establish peptides for which the differences in D-uptake measured in the absence and presence of ligand are significant (Table S3, Supplementary Data). Overall, the HDX results indicate that the binding of CD-grease to TcdA-A2 does not lead to a simple pattern of protection in all of the peptides where intermolecular H-bonds are observed in the crystal structure. Additionally, and unlike the two other protein-carbohydrate complexes considered in this work, ligand binding to TcdA-A2 led to both regions of increased and decreased protection. In Figure 4b, the ΔD_i values are mapped onto the crystal structure of the (TcdA-A2 + 2CD-grease) complex and highlighted in red (protected) and dark blue (de-protected).

Importantly, none of the peptides associated with *site 2* exhibited protection in the presence of CD-grease. Also, peptides 111-120, 117-135 and 121-147, which contain residues N119, S121 and K122 that, based on X-ray data, interact with the ligand in *site 1* exhibited no change in protection upon binding with CD-grease. However, the two overlapping peptides 85-107 and 96-107 (with distinct retention times, 6.2 min and 4.6 min, respectively) did exhibit positive ΔD_i values. These two peptides contain three residues (D92, Q99 and R102) that are predicted, based on the crystal structure, to interact directly with CD-grease in *site 1*. This result is, therefore, consistent with ligand binding to *site 1* under the experimental conditions used. A number of peptic peptides (31-48, 31-55, 158-167, 183-198, 199-207 and 208-225) exhibited

negative ΔD_i values (as large as -3.9 Da), indicating an increase in D-uptake upon ligand binding. It can be seen in Figure 4b that the de-protected regions are mainly located close to the N-terminus, which is the artificial truncation point of the fragment [40]. Notably, changes in D-uptake rates at residues remote from the binding sites have been demonstrated previously for protein-carbohydrate complexes [27, 29], as well as other protein-ligand interactions [54-56]. Both decreases [27, 54, 55] and increases [27, 29, 55, 56] in the D-uptake outside of binding sites have been observed. These data suggest that changes in the structure or dynamics of the N-terminal region of the TcdA-A2 fragment may occur upon binding of CD-grease. Interestingly, no such ligand-induced structural changes are evident from x-ray crystallography data [40]. It is also possible that ligand binding leads to a depopulation of some of the conformers, as this also can influence HDX rates [17].

Influence of protein-carbohydrate interactions on deuterium exchange rates

Several general conclusions regarding the relationship between the nature of protein-carbohydrate interactions and the measured changes in the exchange rates can be drawn from the results of this study. Intermolecular H-bonds between the ligand and backbone amides generally lead to a decrease in D-uptake. Notably, this observation is consistent with those reported previously for other protein-carbohydrate complexes [28]. That protection is also conferred by water-mediated H-bonds involving backbone amides, has not, to our knowledge, been previously reported for protein-carbohydrate interactions, although it was demonstrated for other non-covalent protein complexes [51, 52]. As an example, for the CTB_5 interaction with GM_1-os, positive ΔD_i values were observed for peptides containing residues H13 (direct H-bond with ligand) and G33 (water mediated H-bond). In contrast, putative intermolecular H-bonds involving backbone carbonyl oxygens or side chains did not always lead to protection. For

example, residues D16, D17, D18, T21 and E28 of $Stx1B_5$ participate in direct H-bonds with Pk through their side chains (Table 1). However, based on HDX-MS results, only residues D16, D17 and D18 in peptide 12-20 were protected, while T21 and E28, which are contained in peptide 20-31, were unaffected by ligand binding. It should be emphasized that this analysis is predicated on the assumption that all of the carbohydrate binding sites identified by X-ray crystallography are extensively populated under the solution conditions investigated.

Conclusions

In summary, the application of HDX-MS to localize ligand binding sites for three model carbohydrate-binding proteins is described. Comparison of the differences in D-uptake for peptic peptides produced in the absence and presence of native carbohydrate ligand revealed regions of the protein that are protected against deuterium exchange upon ligand binding. Notably, for all three proteins, the peptides exhibiting protection contain residues known to make up the carbohydrate binding sites, as identified by X-ray crystallography. For the interaction between CTB_5 and GM_1-os, peptides associated with each of the four loops in the CTB monomer that make up the GM_1 binding site were found to exhibit protection against exchange upon ligand binding. For the interaction between $Stx1B_5$ and Pk-OH, peptides containing residues associated with each of the three ligand binding sites were also found to exhibit protection in the presence of ligand. However, because the peptides exhibiting protection include amino acid residues that belong to all three sites (*sites 1, 2 and 3*), it was not possible to establish unambiguously whether all three sites were occupied under the experimental conditions investigated. For the interaction between TcdA-A2 and CD-grease, one (*site 1*) of the two known binding sites was identified based on the observation of protection against exchange in the presence of ligand. However, ligand binding was also found to induce changes in either the structure or the dynamics of the

protein that resulted in significant de-protection of the peptic peptides associated with the N-terminus of the protein. Taken together, the results of this study suggest that HDX-MS can serve as a useful tool for localizing the ligand binding sites in carbohydrate-binding proteins. However, a detailed interpretation of the changes in deuterium exchange upon ligand binding can be challenging due to the presence of ligand-induced changes in protein structure and dynamics.

Acknowledgements

The authors are grateful to the Natural Sciences and Engineering Research Council of Canada and the Alberta Glycomics Centre for financial support and to Prof. G. Armstrong (University of Calgary) for providing $Stx1B_5$.

References

1 Vuignier, K., Schappler, J., Veuthey, J. L., Carrupt, P. A., Martel, S.: Drug-protein binding: A critical review of analytical tools. *Anal. Bioanal. Chem.* **398**, 53-66 (2010)

2 Lee, Y. C., Lee, R. T.: Cabohydrate-protein interactions: Basis of glycobiology. *Accounts Chem. Res.* **28**, 321-327 (1995)

3 Holgersson, J., Gustafsson, A., Breimer, M. E.: Characteristics of protein-carbohydrate interactions as a basis for developing novel carbohydrate-based antirejection therapies. *Immunol. Cell Biol.* **83**, 694-708 (2005)

4 Kamiya, Y., Yagi-Utsumi, M., Yagi, H., Kato, K.: Structural and molecular basis of carbohydrate-protein interaction systems as potential therapeutic targets. *Curr. Pharm. Design* **17**, 1672-1684 (2011)

5 Duan, X. Q., Hall, J. A., Nikaido, H., Quiocho, F. A.: Crystal structures of the maltodextrin/maltose-binding protein complexed with reduced oligosaccharides: Flexibility of tertiary structure and ligand binding. *J. Mol. Biol.* **306**, 1115-1126 (2001)

6 Duan, X. Q., Quiocho, F. A.: Structural evidence for a dominant role of nonpolar interactions in the binding of a transport/chemosensory receptor to its highly polar ligands. *Biochemistry* **41**, 706-712 (2002)

7 Fernandez-Alonso, M. D., Diaz, D., Berbis, M. A., Marcelo, F., Canada, J., Jimenez-Barbero, J.: Protein-carbohydrate interactions studied by NMR: From molecular recognition to drug design. *Curr. Protein Pept. Sci.* **13**, 816-830 (2012)

8 Kohn, J. E., Afonine, P. V., Ruscio, J. Z., Adams, P. D., Head-Gordon, T.: Evidence of functional protein dynamics from X-ray crystallographic ensembles. *PLoS Comput. Biol.* **6**, e1000911 (2010)

9 Percy, A. J., Rey, M., Burns, K. M., Schriemer, D. C.: Probing protein interactions with hydrogen/deuterium exchange and mass spectrometry-A review. *Anal. Chim. Acta* **721**, 7-21 (2012)

10 Chalmers, M. J., Busby, S. A., Pascal, B. D., West, G. M., Griffin, P. R.: Differential hydrogen/deuterium exchange mass spectrometry analysis of protein-ligand interactions. *Expert Rev. Proteomics* **8**, 43-59 (2011)

11 Iacob, R. E., Engen, J. R.: Hydrogen exchange mass spectrometry: Are we out of the quicksand? *J. Am. Soc. Mass Spectrom.* **23**, 1003-1010 (2012)

12 Garcia, R. A., Pantazatos, D., Villarreal, F. J.: Hydrogen/deuterium exchange mass spectrometry for investigating protein-ligand interactions. *Assay Drug Dev. Technol.* **2**, 81-91 (2004)

13 Houde, D., Berkowitz, S. A., Engen, J. R.: The utility of hydrogen/deuterium exchange mass spectrometry in biopharmaceutical comparability studies. *J. Pharm. Sci.* **100**, 2071-2086 (2011)

14 Zhang, Z. Q., Smith, D. L.: Determination of amide hydrogen exchange by mass spectrometry: A new tool for protein-structure elucidation. *Protein Sci.* **2**, 522-531 (1993)

15 Pacholarz, K. J., Garlish, R. A., Taylor, R. J., Barran, P. E.: Mass spectrometry based tools to investigate protein-ligand interactions for drug discovery. *Chem. Soc. Rev.* **41**, 4335-4355 (2012)

16 Huang, R. Y. C., Wen, J., Blankenship, R. E., Gross, M. L.: Hydrogen-deuterium exchange mass spectrometry reveals the interaction of Fenna-Matthews-Olson protein and chlorosome CsmA protein. *Biochemistry* **51**, 187-193 (2012)

17 Wildes, D., Marqusee, S.: Hydrogen exchange and ligand binding: Ligand-dependent and ligand-independent protection in the Src SH3 domain. *Protein Sci.* **14**, 81-88 (2005)

18 Zhang, J., Chalmers, M. J., Stayrook, K. R., Burris, L. L., Garcia-Ordonez, R. D., Pascal, B. D., Burris, T. P., Dodge, J. A., Griffin, P. R.: Hydrogen/deuterium exchange reveals distinct agonist/partial agonist receptor dynamics within vitamin D receptor/retinoid X receptor heterodimer. *Structure* **18**, 1332-1341 (2010)

19 Chetty, P. S., Mayne, L., Kan, Z. Y., Lund-Katz, S., Englander, S. W., Phillips, M. C. Apolipoprotein A-I helical structure and stability in discoidal high-density lipoprotein (HDL) particles by hydrogen exchange and mass spectrometry. *Proc. Natl. Acad. Sci. U.S.A.* **109**, 11687-11692 (2012)

20 Ahn, J., Engen, J. R.: The use of hydrogen/deuterium exchange mass spectrometry in epitope mapping. *Chim. Oggi-Chem. Today* **31**, 25-28 (2013)

21 Jorgensen, T. J. D., Gardsvoll, H., Dano, K., Roepstorff, P., Ploug, M.: Dynamics of urokinase receptor interaction with peptide antagonists studied by amide hydrogen exchange and mass spectrometry. *Biochemistry* **43**, 15044-15057 (2004)

22 Dai, S. Y., Burris, T. P., Dodge, J. A., Montrose-Rafizadeh, C., Wang, Y., Pascal, B. D., Chalmers, M. J., Griffin, P. R.: Unique ligand binding patterns between estrogen receptor alpha and beta revealed by hydrogen-deuterium exchange. *Biochemistry* **48**, 9668-9676 (2009)

23 Hamuro, Y., Coales, S. J., Morrow, J. A., Molnar, K. S., Tuske, S. J., Southern, M. R., Griffin, P. R.: Hydrogen/deuterium-exchange (H/D-Ex) of PPAR gamma LBD in the presence of various modulators. *Protein Sci.* **15**, 1883-1892 (2006)

24 Wei, H., Ahn, J., Yu, Y. Q., Tymiak, A., Engen, J. R., Chen, G. D.: Using hydrogen/deuterium exchange mass spectrometry to study conformational changes in granulocyte colony stimulating factor upon PEGylation. *J. Am. Soc. Mass. Spectrom.* **23**, 498-504 (2012)

25 Pan, Y., Brown, L., Konermann, L.: Hydrogen exchange mass spectrometry of bacteriorhodopsin reveals light-induced changes in the structural dynamics of a biomolecular machine. *J. Am. Chem. Soc.* **133**, 20237-20244 (2011)

26 Pan, Y., Piyadasa, H., O'Neil, J. D., Konermann, L.: Conformational dynamics of a membrane transport protein probed by H/D exchange and covalent labeling: The glycerol facilitator. *J. Mol. Biol.* **416**, 400-413 (2012)

27 King, D., Bergmann, C., Orlando, R., Benen, J. A. E., Kester, H. C. M., Visser, J.: Use of amide exchange mass spectrometry to study conformational changes within the endopolygalacturonase II-homogalacturonan-polygalacturonase inhibiting protein system. *Biochemistry* **41**, 10225-10233 (2002)

28 King, D., Lumpkin, M., Bergmann, C., Orlando, R.: Studying protein-carbohydrate interactions by amide hydrogen/deuterium exchange mass spectrometry. *Rapid Commun. Mass Spectrom.* **16**, 1569-1574 (2002)

29 Seyfried, N. T., Atwood, J. A., Yongye, A., Almond, A., Day, A. J., Orlando, R., Woods, R. J.: Fourier transform mass spectrometry to monitor hyaluronan-protein interactions: Use of hydrogen/deuterium amide exchange. *Rapid Commun. Mass Spectrom.* **21**, 121-131 (2007)

30 Huzil, J. T., Chik, J. K., Slysz, G. W., Freedman, H., Tuszynski, J., Taylor, R. E., Sackett, D. L., Schriemer, D. C.: A unique mode of microtubule stabilization induced by peloruside A. *J. Mol. Biol.* **378**, 1016-1030 (2008)

31 Henkels, C. H., Oas, T. G.: Ligation-State Hydrogen Exchange: Coupled Binding and Folding Equilibria in Ribonuclease P Protein. *J. Am. Chem. Soc.* **128**, 7772-7781 (2006)

32 Sowole, M. A., Konermann, L.: Effects of Protein−Ligand Interactions on Hydrogen/Deuterium Exchange Kinetics: Canonical and Noncanonical Scenarios. *Anal. Chem.* **86**, 6715-6722 (2014)

33 Lee, C. T., Graf, C., Mayer, F. J., Richter, S. M., Mayer, M. P.: Dynamics of the regulation of Hsp90 by the co-chaperone Sti1. *Embo J.* **31**, 1518-1528 (2012)

34 Bennett, M. J., Barakat, K., Huzil, J. T., Tuszynski, J., Schriemer, D. C.: Discovery and characterization of the laulimalide-microtubule binding mode by mass shift perturbation mapping. *Chem. Biol.* **17**, 725-734 (2010)

35 Lin, H., Kitova, E. N., Klassen, J. S.: Measuring positive cooperativity using the direct ESI-MS assay. Cholera toxin B subunit homopentamer binding to GM1 pentasaccharide. *J. Am. Soc. Mass Spectrom.* **25**, 104-110 (2014)

36 Merritt, E. A., Merritt, E. A., Sarfaty, S., Jobling, M. G., Chang, T., Holmes, R. K., Hirst, T. R., Hol, W. G. J.: Structural studies of receptor binding by cholera toxin mutants. *Protein Sci.* **6**, 1516-1528 (1997)

37 Ling, H., Ling, H., Boodhoo, A., Hazes, B., Cummings, M. D., Armstrong, G. D., Brunton, J. L., Read, R. J.: Structure of the Shiga-like toxin I B-pentamer complexed with an analogue of its receptor Gb_3. *Biochemistry* **37**, 1777-1788 (1998)

38 Johannes, L., Romer, W.: Shiga toxins - from cell biology to biomedical applications. *Nat. Rev. Microbiol.* **8**, 105-116 (2010)

39 Stein, P. E., Boodhoo, A., Tyrrell, G. J., Brunton, J. L., Read, R. J.: Crystal structure of the cell-binding B oligomer of verotoxin-1 from *E. coli*. *Nature* **355**, 748-750 (1992)

40 Greco, A., Ho, J. G. S., Lin, S. J., Palcic, M. M., Rupnik, M., Ng, K. K. S.: Carbohydrate recognition by *Clostridium difficile* toxin A. *Nat. Struct. Mol. Biol.* **13**, 460-461 (2006)

41 Dingle, T., Wee, S., Mulvey, G. L., Greco, A., Kitova, E. N., Sun, J. X., Lin, S. J., Klassen, J. S., Palcic, M. M., Ng, K. K. S., Armstrong, G. D.: Functional properties of the carboxy-terminal host cell-binding domains of the two toxins, TcdA and TcdB, expressed by *Clostridium difficile*. *Glycobiology* **18**, 698-706 (2008)

42 Glasoe, P. K., Long, F. A. Use of glass electrods to measure acidities in deuterium oxide. *J. Phys. Chem*. **64**, 188-189 (1960)

43 Wales, T. E., Eggertson, M. J., Engen, J. R.: Considerations in the analysis of hydrogen exchange mass spectrometry data. *Methods Mol. Biol.* **1007**, 263-288 (2013)

44 Keppel, T. R., Howard, B. A., Weis, D. D.: Mapping unstructured regions and synergistic folding in intrinsically disordered proteins with amide H/D exchange mass spectrometry. *Biochemistry* **50**, 8722-8732 (2011)

45 Sheff, J. G., Rey, M., Schriemer, D. C.: Peptide-column interactions and their influence on back exchange rates in hydrogen/deuterium exchange-MS. *J. Am. Soc. Mass Spectrom.* **24**, 1006-1015 (2013)

46 Majumdar, R., Manikwar, P., Hickey, J. M., Samra, H. S., Sathish, H. A., Bishop, S. M., Middaugh, C. R., Volkin, D. B., Weis, D. D.: Effects of salts from the Hofmeister series

on the conformational stability, aggregation propensity, and local flexibility of an IgG1 monoclonal antibody. *Biochemistry* **52**, 3376-3389 (2013)

47 Liu, S., Liu, L., Uzuner, U., Zhou, X., Gu, M., Shi, W., Zhang, Y., Dai, S. Y., Yuan, J. S. HDX-Analyzer: a novel package for statistical analysis of protein structure dynamics. *BMC Bioinformatics* **12** (Suppl 1**)**, S43 (2011)

48 Li, Z., Huang, R. Y., Yopp, D. C., Hileman, T. H., Santangelo, T. J., Hurwitz, J., Hudgens J. W., Kelman, Z.: A novel mechanism for regulating the activity of proliferating cell nuclear antigen by a small protein. *Nucleic Acids Res.* **42**, 5776-5789 (2014)

49 Merritt, E. A., Sarfaty, S., Vandenakker, F., Lhoir, C., Martial, J. A., Hol, W. G. J.: Crystal-structure of cholera toxin B-pentamer bound to Receptor G_{M1} pentasaccharide. *Protein Sci.* **3**, 166-175 (1994)

50 Merritt, E. A., Kuhn, P., Sarfaty, S., Erbe, J. L., Holmes, R. K., Ho, W. G. J.: The 1.25 angstrom resolution refinement of the cholera toxin B-pentamer: Evidence of peptide backbone strain at the receptor-binding site. *J. Mol. Biol.* **282**, 1043-1059 (1998)

51 Skinner, J. J., Lim, W. K., Bedard, S., Black, B. E., Englander, S. W.: Protein dynamics viewed by hydrogen exchange. *Protein Sci.* **21**, 996-1005 (2012)

52 Zhang, J., Chalmers, M. J., Stayrook, K. R., Burris, L. L., Garcia-Ordonez, R. D., Pascal, B. D., Burris, T. P., Dodge, J. A., Griffin, P. R.: Hydrogen/deuterium exchange reveals distinct agonist/partial agonist receptor dynamics within vitamin D receptor/retinoid X receptor heterodimer. *Structure* **18**, 1332-1341 (2010)

53 Shimizu, H., Field, R. A., Homans, S. W., Donohue-Rolfe, A.: Solution structure of the complex between the B-subunit homopentamer of verotoxin VT-1 from Escherichia coli

and the trisaccharide moiety of globotriaosylceramide. *Biochemistry* **37**, 11078-11082 (1998)

54 Benjamin, D. C., Williams, D. C. Jr, Smith-Gill, S. J., Rule, G. S.: Long-range changes in a protein antigen due to antigen-antibody interaction. *Biochemistry* **31**, 9539-9545 (1992)

55 Sowole, M. A., Alexopoulos, J. A., Cheng, Y.Q., Ortega, J., Konermann, L. Activation of ClpP protease by ADEP antibiotics: insights from hydrogen exchange mass spectrometry. *J. Mol. Biol.* **425**, 4508-4519 (2013)

56 Resetca, D., Haftchenary, S., Gunning, P. T., Wilson, D. J. Changes in signal transducer and activator of transcription 3 (STAT3) dynamics induced by complexation with pharmacological inhibitors of Src homology 2 (SH2) domain dimerization. *J. Biol. Chem.* **289**, 32538-32547 (2014)

Table 1. Summary of the intermolecular H-bonds identified in the crystal structures of the three model protein-carbohydrate complexes: (CTB_5 + $5GM_1$-os), PDB ID 3CHB;[50] ($Stx1B_5$ + 15Pk), PDB ID 1BOS;[37] and (TcdA-A2 + 2CD-grease), PDB ID 2G7C.[40]

Protein-carbohydrate complex	**Amino acid residues that participate in H-bonds with the carbohydrate ligands** [a]
(CTB_5 + $5GM_1$-os)	E11(O), H13(N, ND1), G33 (N),[b,c] E51(OE1), Q56(O), Q61(NE2), N90(OD1, ND2) and K91(NZ)
($Stx1B_5$ + 15Pk)	Site 1: D17(OD2), T21(OG1), E28(OE2), G60(N, O) Site 2: D16(OD2),[c] N32(N, OD1), R33(NH2, NE), N55(N, OD1) and F63(N, O) Site 3: D18(OD1, OD2),[c] W34(N) and N35(N)
(TcdA-A2 + 2CD-grease)	Site 1: D92(OD2), Q99(NE2), R102(N), N119(O), S121(OG) and K122(NZ) Site 2: D183(OD2), Q190(NE2), R193(N), N210(O), S212(OG) and K213(NZ)

a. Specific atoms of the amino acid residue that participate in the intermolecular H-bonds. b. Water mediated H-bond between the specified residue and ligand. c. H-bond involves residue from an adjacent subunit.

Figure captions

Figure 1. Protein-carbohydrate complexes considered for HDX-MS analysis: (a) (CTB_5 + $5GM_1$-os) complex (each subunit has one GM_1-os binding site), PDB ID 3CHB,[50] (b) ($Stx1B_5$ + 15Pk) complex (each subunit has three Pk binding sites), PDB ID 1BOS,[37] and (c) (TcdA-A2 + 2CD-grease) complex (each TcdA-A2 has two CD-grease binding sites), PDB ID 2G7C.[40] (d) The structures of the carbohydrate ligands, GM_1-os, Pk-OH and CD-grease.

Figure 2. (a) Difference plot of peptide level D-uptake between free CTB_5 and (CTB_5 + $5GM_1$-os) complex for a subset of peptides that cover 96.1% of CTB monomer sequence. The x-axis indicates the position (residue number) of the peptides considered. The y-axis shows the ΔD_i values for each peptide, summed over all of the labeling times. The errors bars correspond to one standard deviation. (b) Cartoon illustration of ΔD_i values mapped onto the crystal structure of the (CTB_5 + $5GM_1$-os) complex (PDB 3CHB). The coloured region corresponds to one representative CT B subunit. The regions highlighted in red (with corresponding residue numbers indicated) exhibited protection from deuterium exchange upon ligand binding, while the regions highlighted in cyan were unaffected by ligand binding.

Figure 3. (a) Difference plot of peptide level D-uptake between free $Stx1B_5$ and ($Stx1B_5$ + 15Pk-OH) complex for a subset of peptides that cover 95.6% of Stx1B monomer sequence. The x-axis indicates the position (residue number) of the peptides considered. The y-axis shows the ΔD_i values for each peptide, summed over all of the labeling times. The errors bars correspond to one standard deviation. (b) Cartoon illustration of ΔD_i values mapped onto the crystal structure of the ($Stx1B_5$ + 15Pk) complex (PDB

1BOS). The coloured region corresponds to one representative Stx1 B subunit. The regions highlighted in red (with corresponding residue numbers indicated) exhibited protection from deuterium exchange upon ligand binding, while the regions highlighted in cyan were unaffected by ligand binding.

Figure 4. (a) Difference plot of peptide level D-uptake between free TcdA-A2 and (TcdA-A2 + 2CD-grease) complex for a subset of peptides that cover 92.4% of the TcdA-A2 sequence. The x-axis indicates the position (residue number) of the peptides considered. The y-axis shows the ΔD_i values for each peptide, summed over all of the labeling times. The errors bars correspond to one standard deviation. (b) Cartoon illustration of ΔD_i values mapped onto the crystal structure of the (TcdA-A2 + 2CD-grease) complex (PDB 2G7C). The regions highlighted in red and dark blue exhibited protection or de-protection, respectively, against deuterium exchange upon ligand binding; the regions shown in cyan were unaffected by ligand binding.

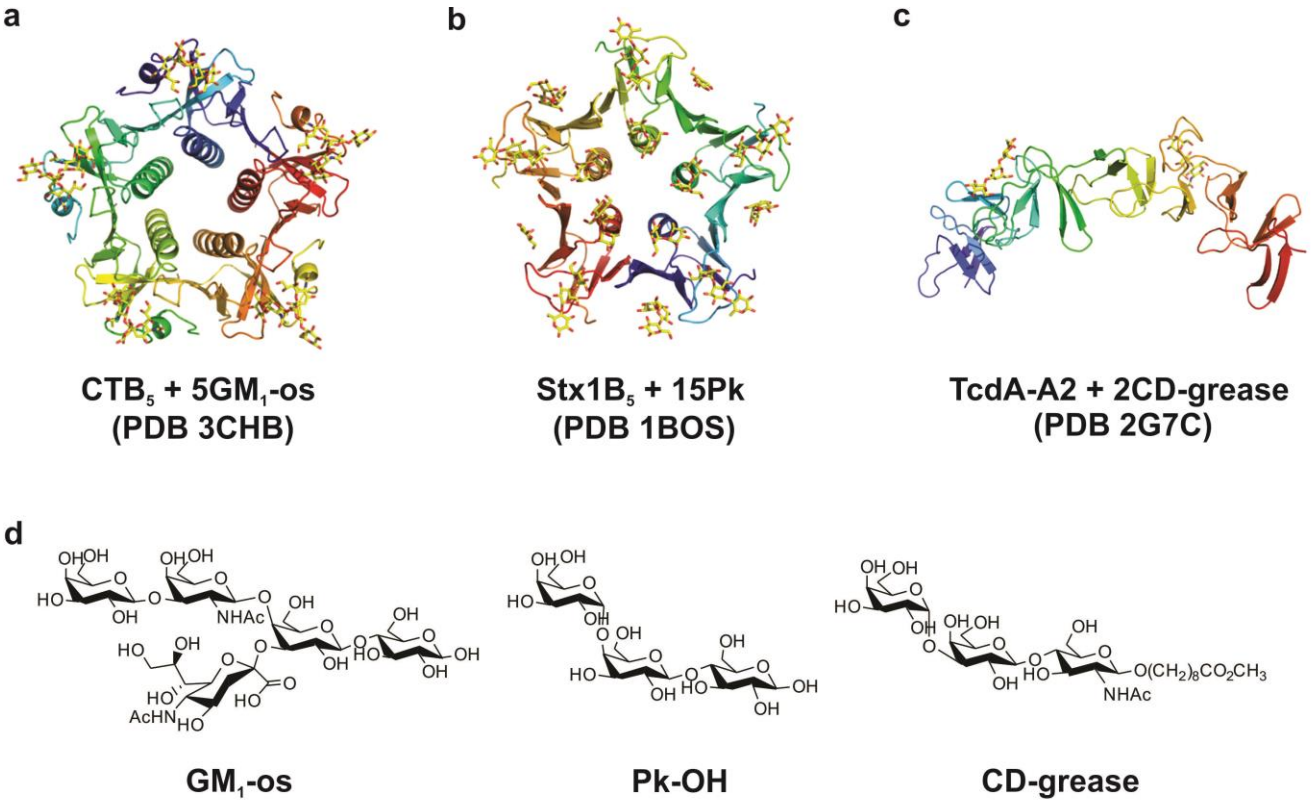
a
b
c
CTB5 + 5GM1-os
(PDB 3CHB)
Stx1B5 + 15Pk
(PDB 1BOS)
TcdA-A2 + 2CD-grease
(PDB 2G7C)
d
GM1-os
Pk-OH
CD-grease

Figure 1

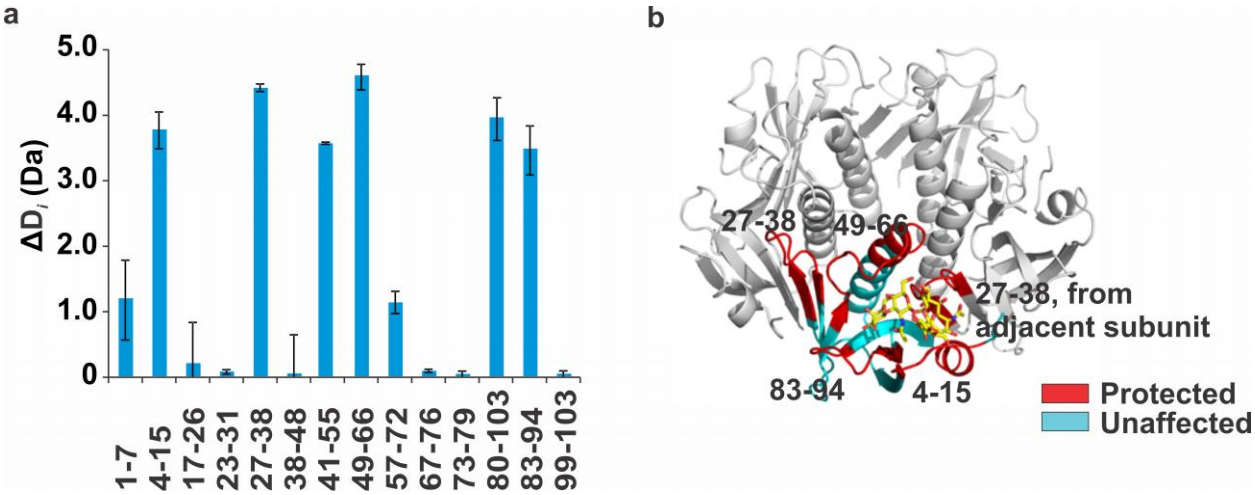
a
5.0
4.0
3.0
2.0
1.0
0
ΔD_i (Da)
1-7
4-15
17-26
23-31
27-38
38-48
41-55
49-66
57-72
67-76
73-79
80-103
83-94
99-103
b
27-38
49-66
27-38, from
adjacent subunit
83-94
4-15
Protected
Unaffected

Figure 2

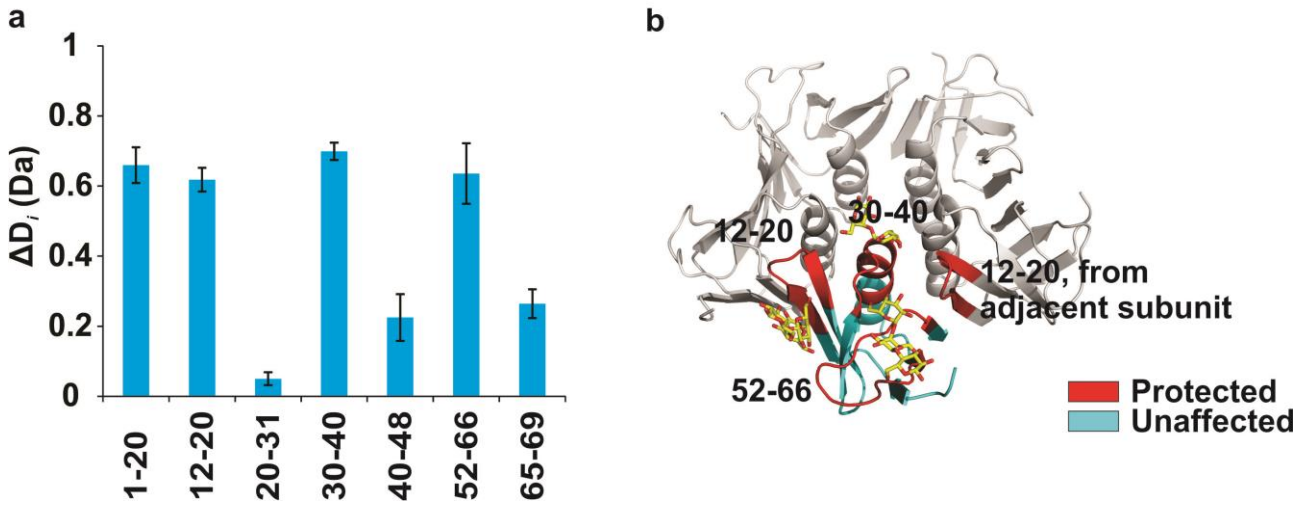
a
1
0.8
0.6
0.4
0.2
0
ΔD_i (Da)
1-20
12-20
20-31
30-40
40-48
52-66
65-69
b
12-20
30-40
12-20, from
adjacent subunit
52-66
Protected
Unaffected

Figure 3

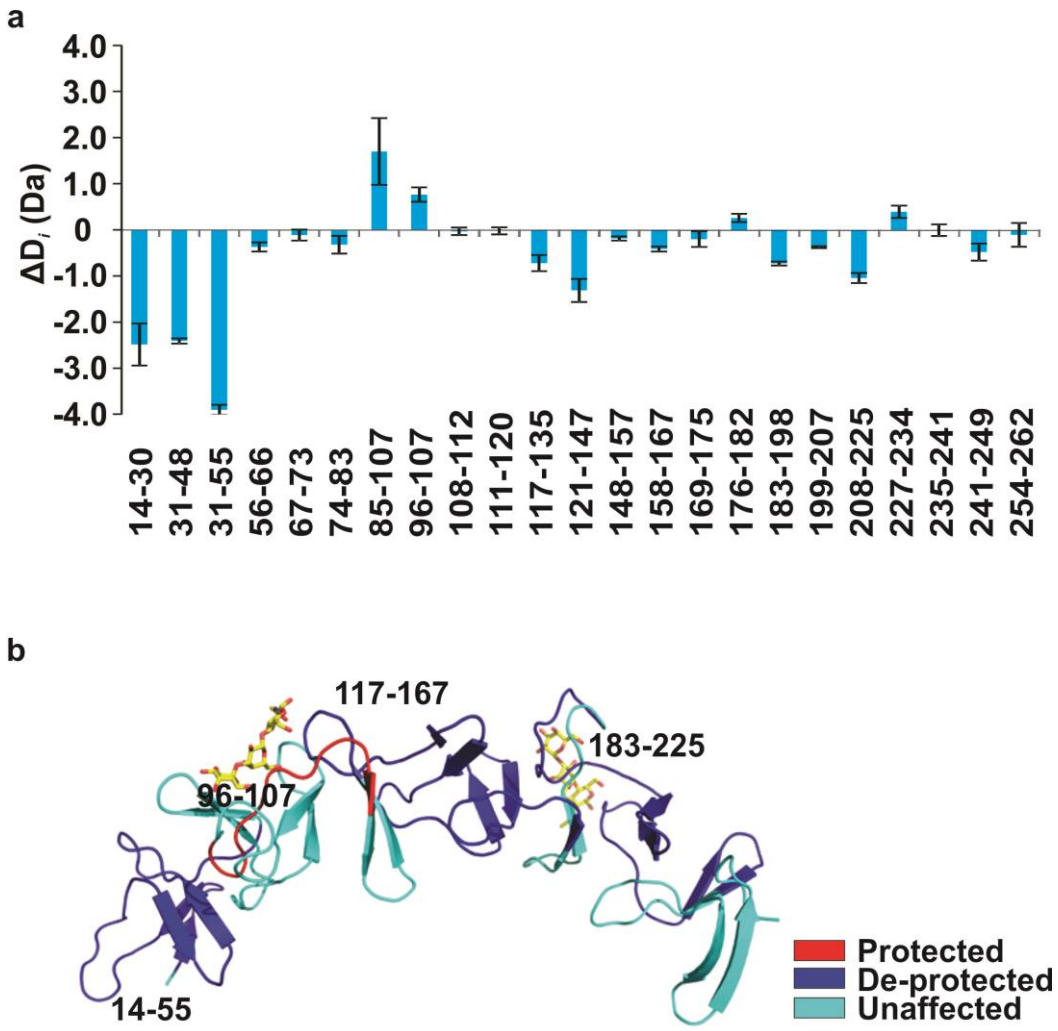
a
4.0
3.0
2.0
1.0
0
-1.0
-2.0
-3.0
-4.0
ΔD_i (Da)
14-30
31-48
31-55
56-66
67-73
74-83
85-107
96-107
108-112
111-120
117-135
121-147
148-157
158-167
169-175
176-182
183-198
199-207
208-225
227-234
235-241
241-249
254-262
b
117-167
183-225
96-107
14-55
Protected
De-protected
Unaffected

Figure 4

Supplementary Data For:

Localizing Carbohydrate Binding Sites in Proteins using Hydrogen/Deuterium Exchange Mass Spectrometry

Jingjing Zhang, Elena N. Kitova, Jun Li, Luiz Eugenio, Kenneth Ng and John S. Klassen

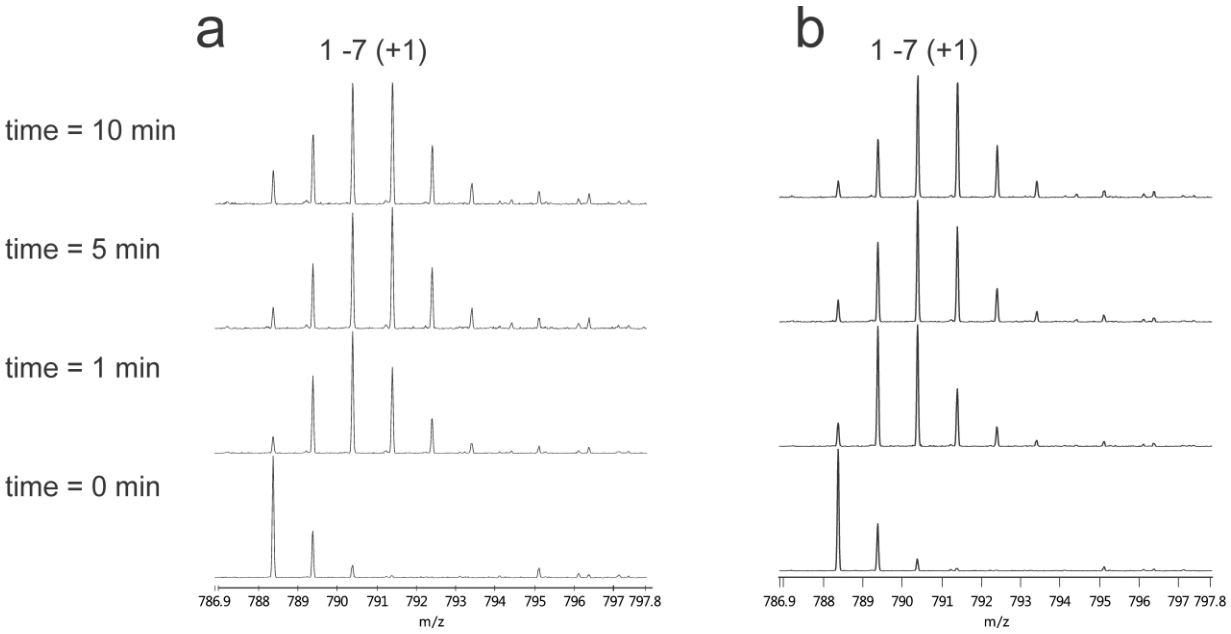

Figure S1. Mass spectra of singly charged ions of peptic peptide 1-7 obtained from (a) free and (b) ligand-bound CTB_5 at deuterium exposure times of 0, 1, 5 and 10 min.

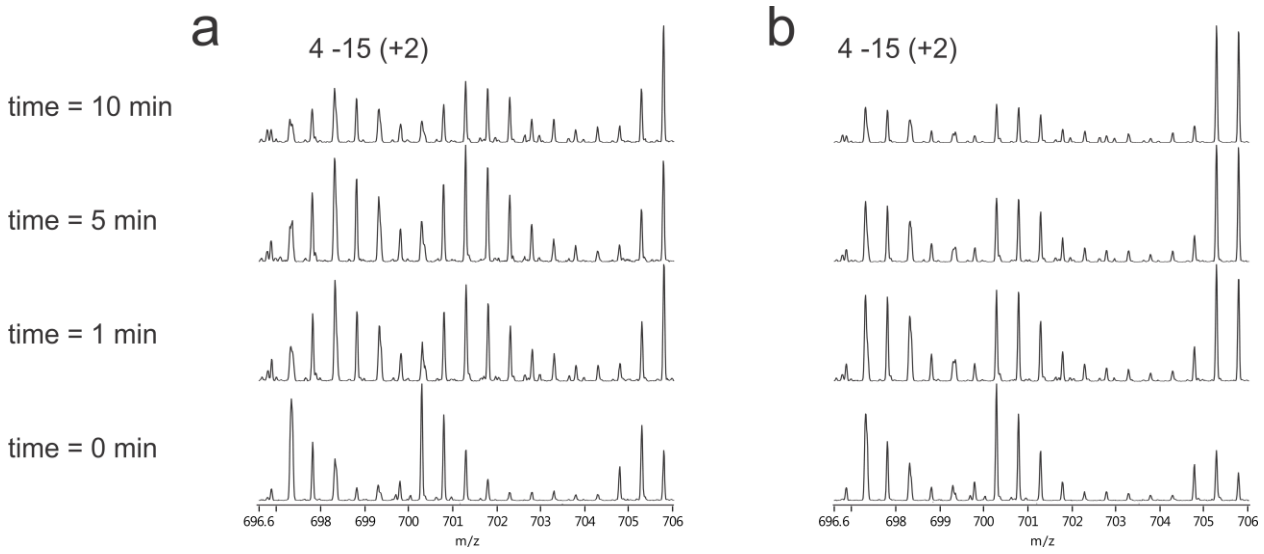

Figure S2. Mass spectra of doubly charged ions of peptic peptide 4-15 obtained from (a) free and (b) ligand-bound CTB_5 at deuterium exposure times of 0, 1, 5 and 10 min.

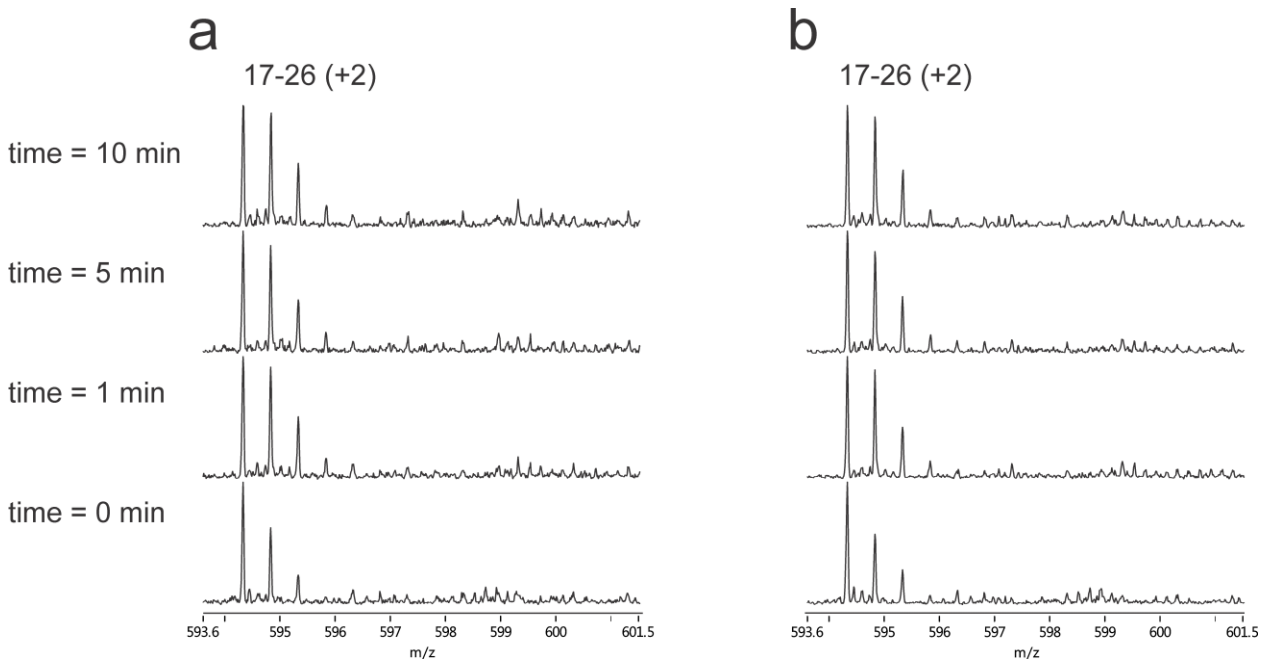

Figure S3. Mass spectra of doubly charged ions of peptic peptide 17-26 obtained from (a) free and (b) ligand-bound CTB_5 at deuterium exposure times of 0, 1, 5 and 10 min.

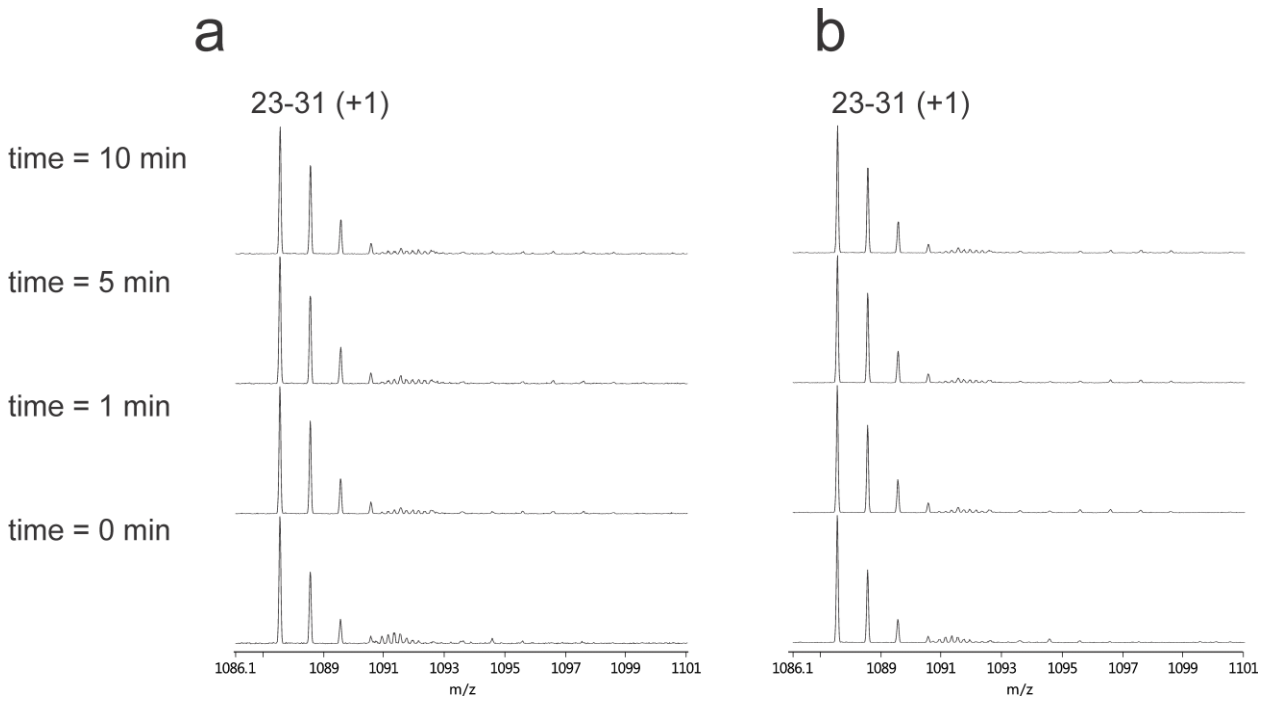

Figure S4. Mass spectra of singly charged ions of peptic peptide 23-31 obtained from (a) free and (b) ligand-bound CTB_5 at deuterium exposure times of 0, 1, 5 and 10 min.

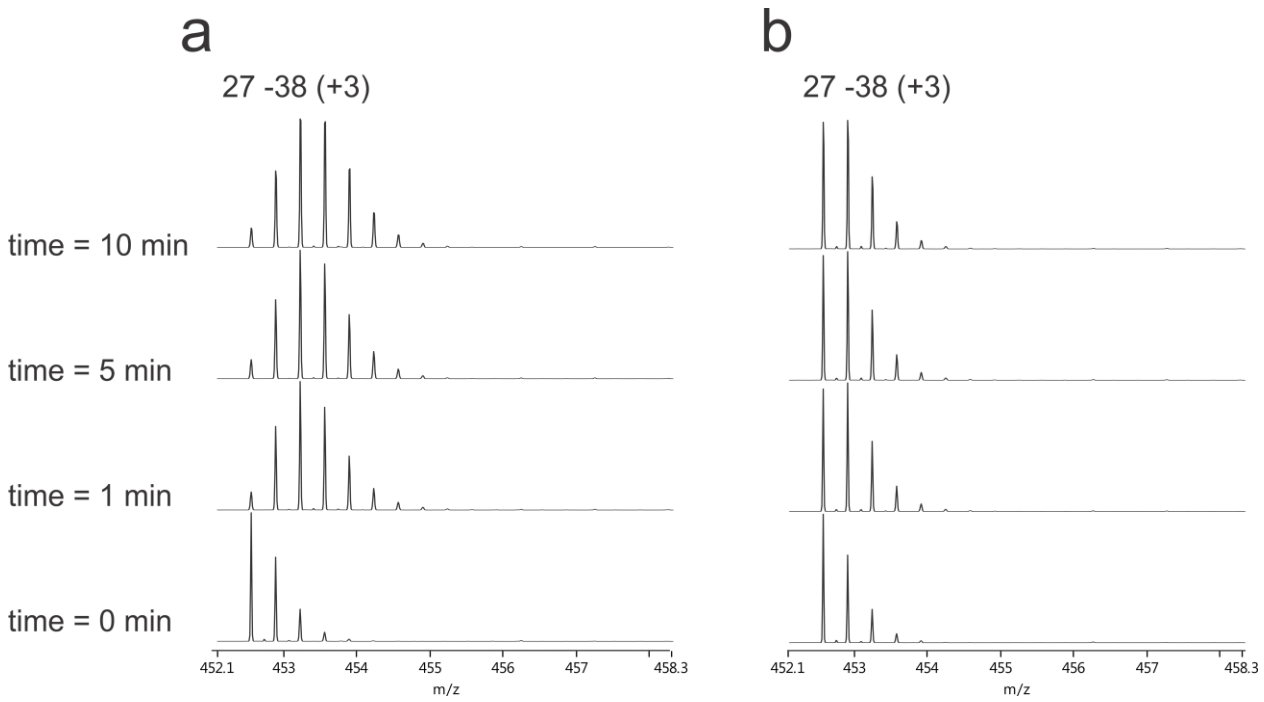

Figure S5. Mass spectra of triply charged ions of peptic peptide 27-38 obtained from (a) free and (b) ligand-bound CTB_5 at deuterium exposure times of 0, 1, 5 and 10 min.

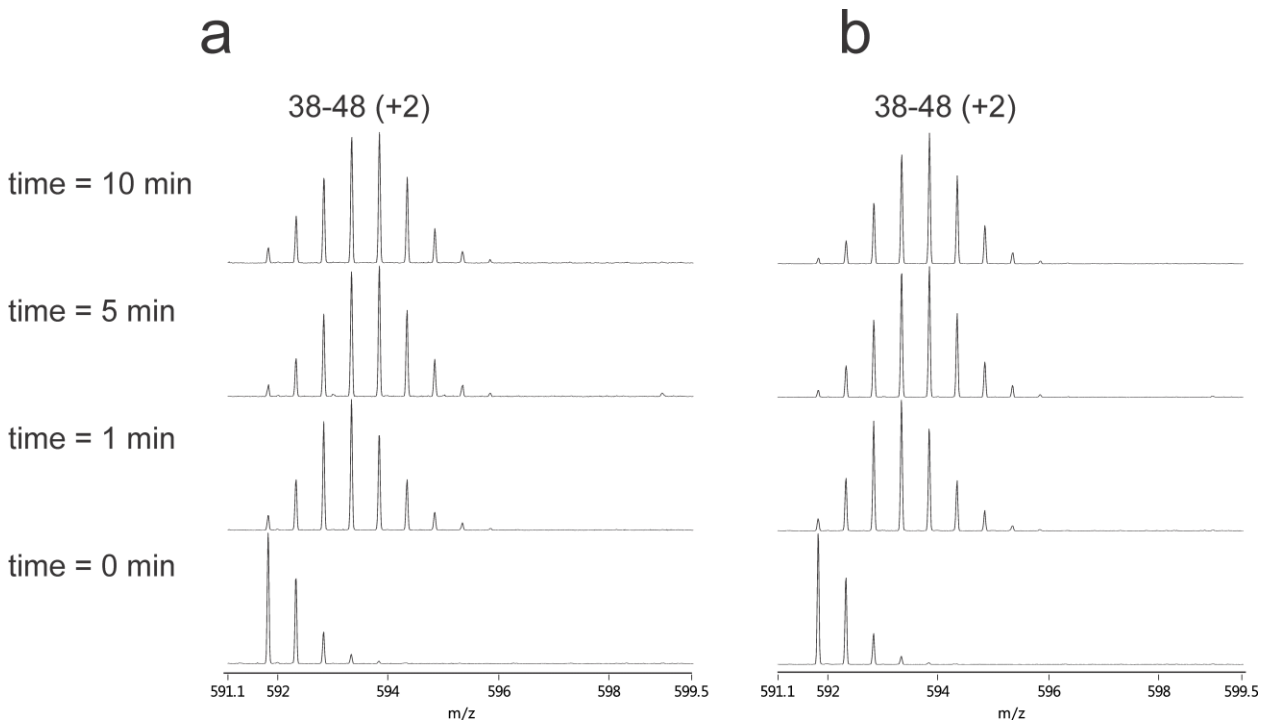

Figure S6. Mass spectra of doubly charged ions of peptic peptide 38-48 obtained from (a) free and (b) ligand-bound CTB_5 at deuterium exposure times of 0, 1, 5 and 10 min.

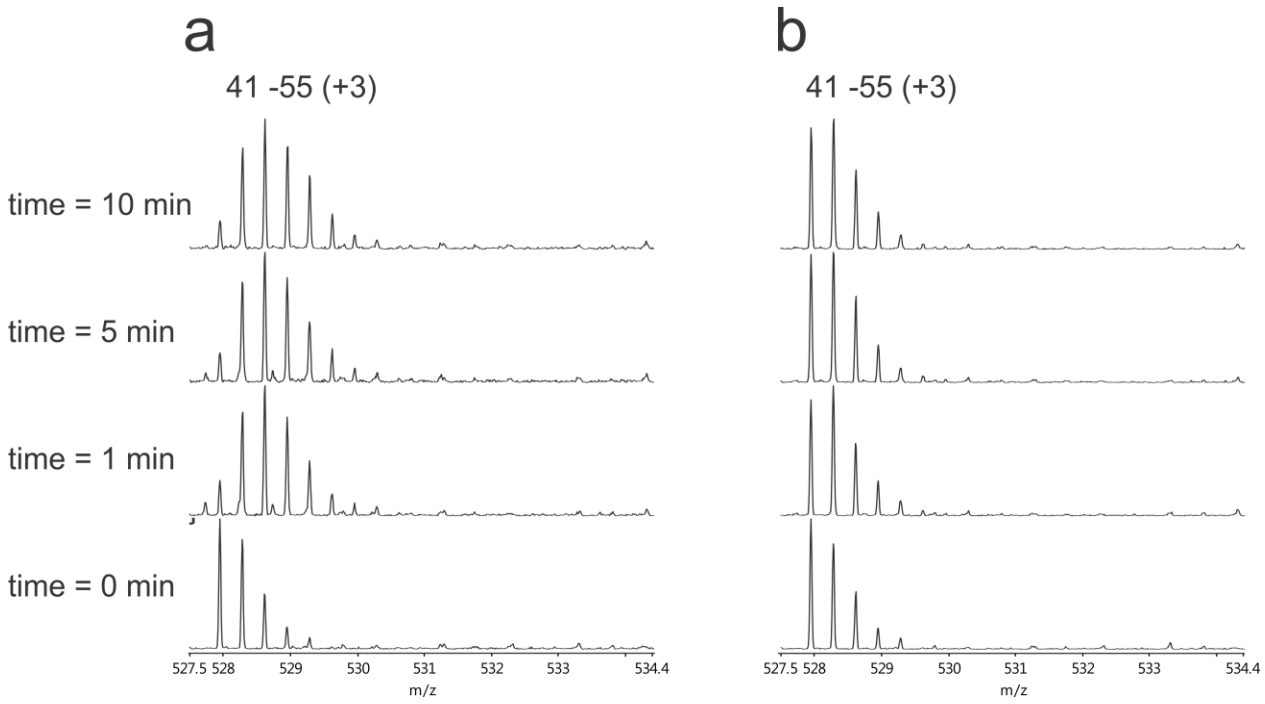

Figure S7. Mass spectra of triply charged ions of peptic peptide 41-55 obtained from (a) free and (b) ligand-bound CTB_5 at deuterium exposure times of 0, 1, 5 and 10 min.

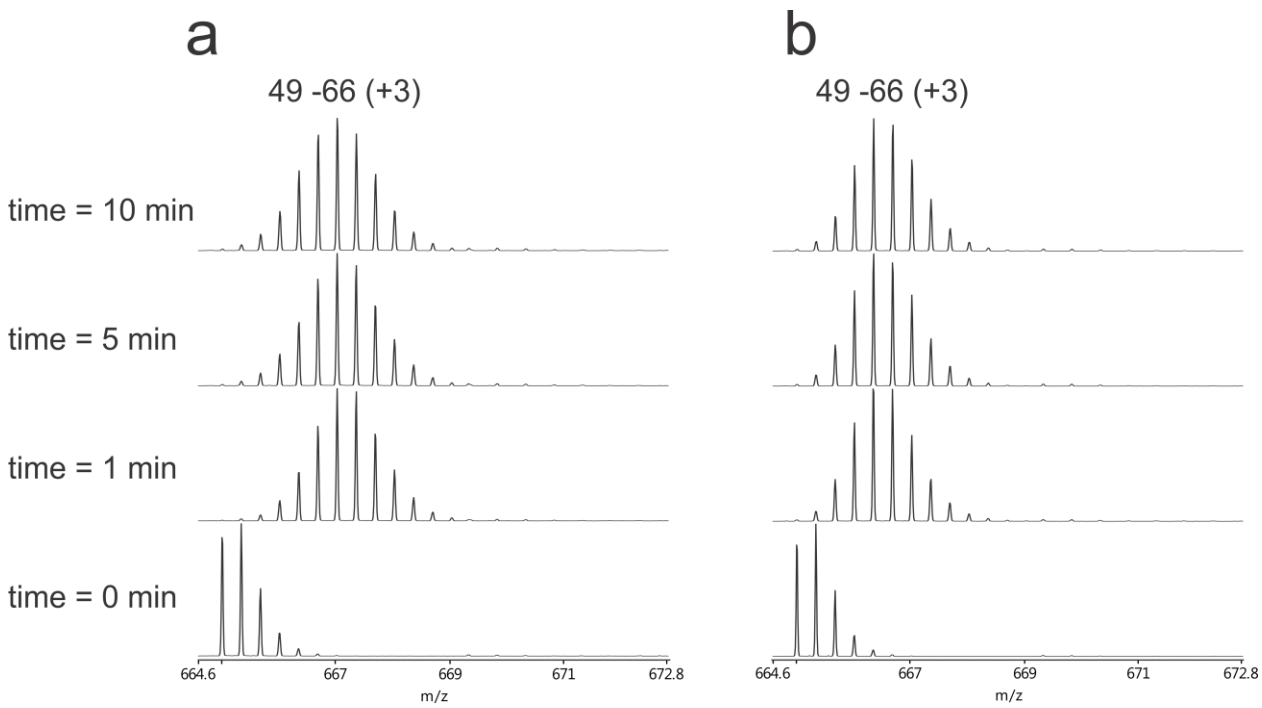

Figure S8. Mass spectra triply charged ions of peptic peptide 49-66 obtained from (a) free and (b) ligand-bound CTB_5 at deuterium exposure times of 0, 1, 5 and 10 min.

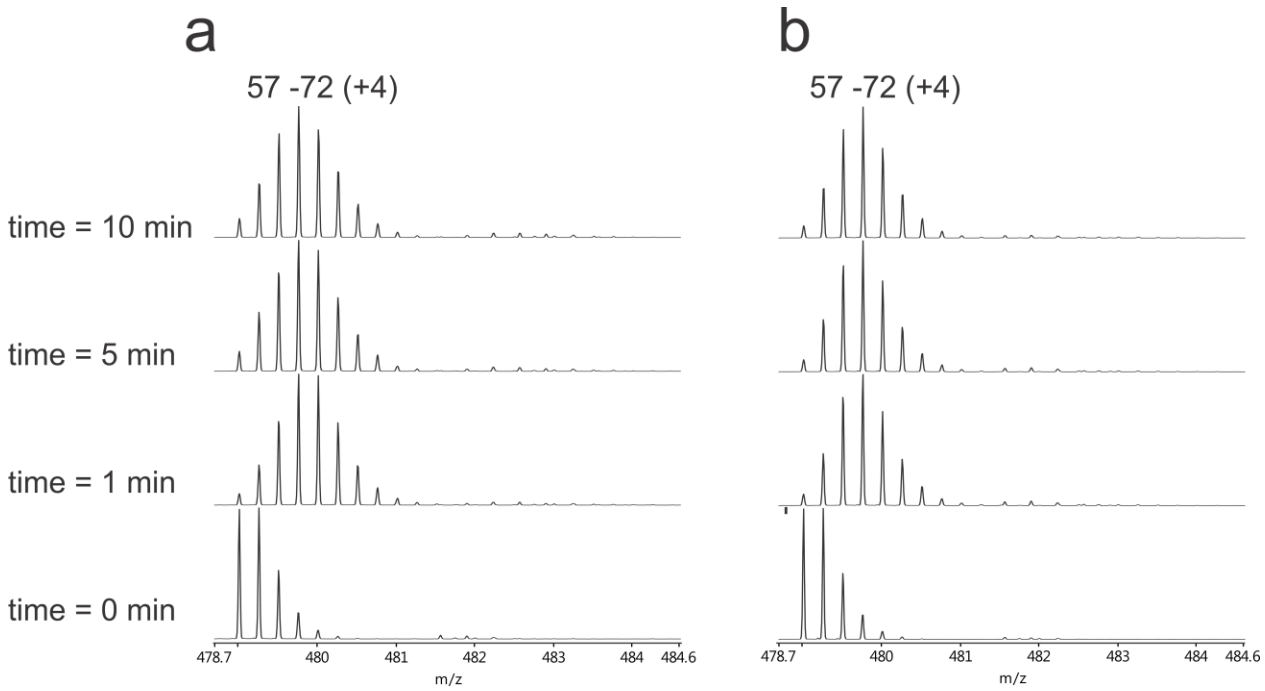

Figure S9. Mass spectra of quadruply charged ions of peptic peptide 57-72 obtained from (a) free and (b) ligand-bound CTB_5 at deuterium exposure times of 0, 1, 5 and 10 min.

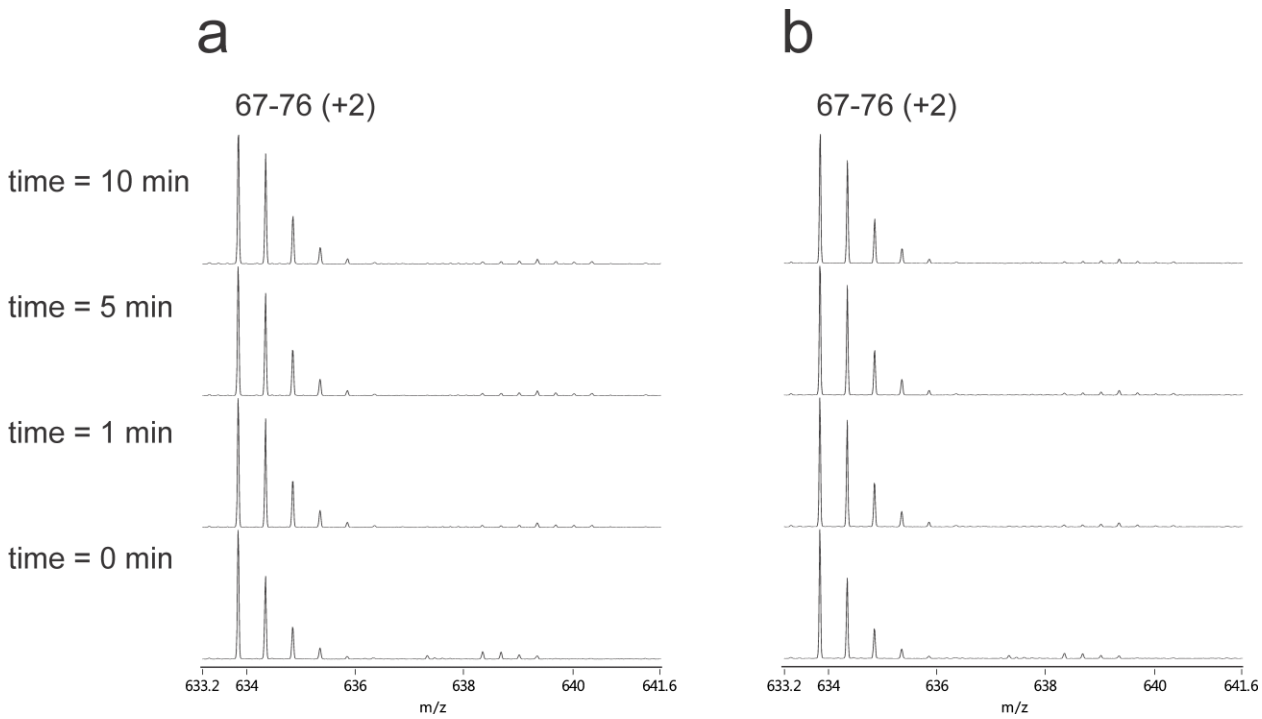

Figure S10. Mass spectra of doubly charged ions of peptic peptide 67-76 obtained from (a) free and (b) ligand-bound CTB_5 at deuterium exposure times of 0, 1, 5 and 10 min.

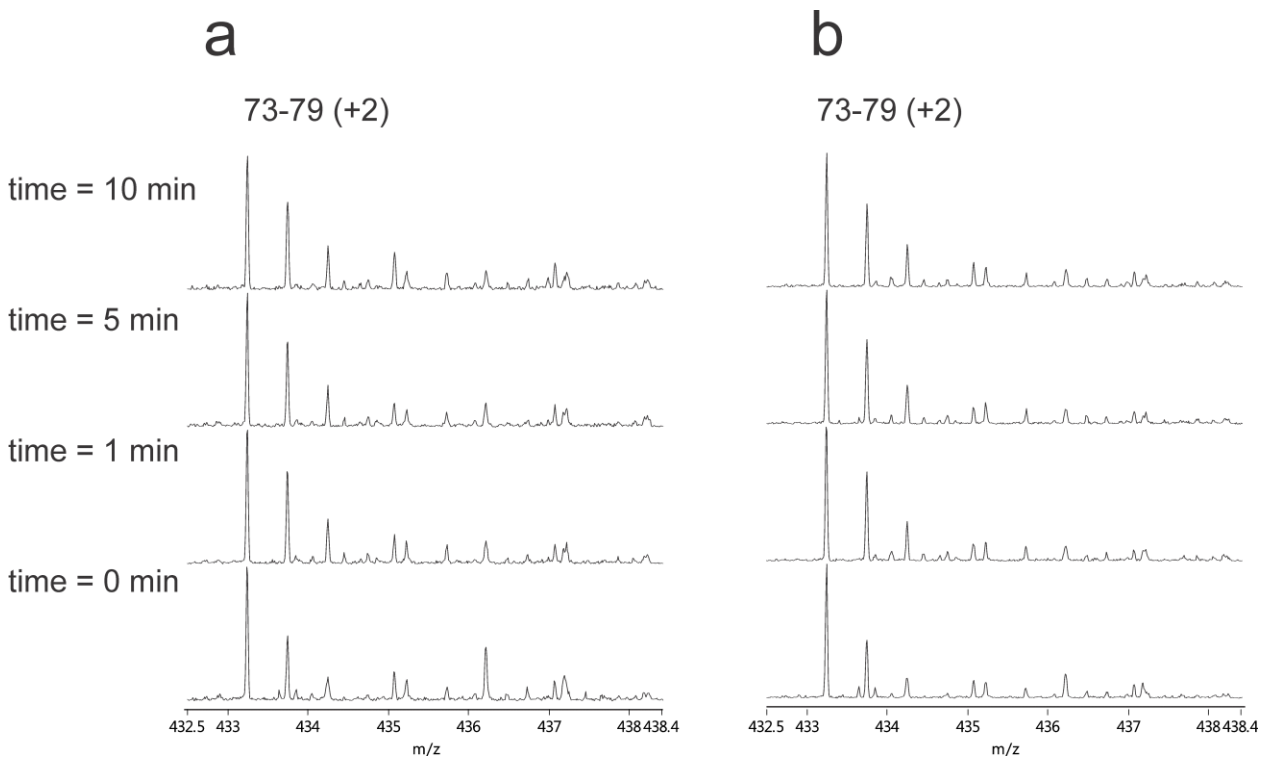

Figure S11. Mass spectra of doubly charged ions of peptic peptide 73-79 obtained from (a) free and (b) ligand-bound CTB_5 at deuterium exposure times of 0, 1, 5 and 10 min.

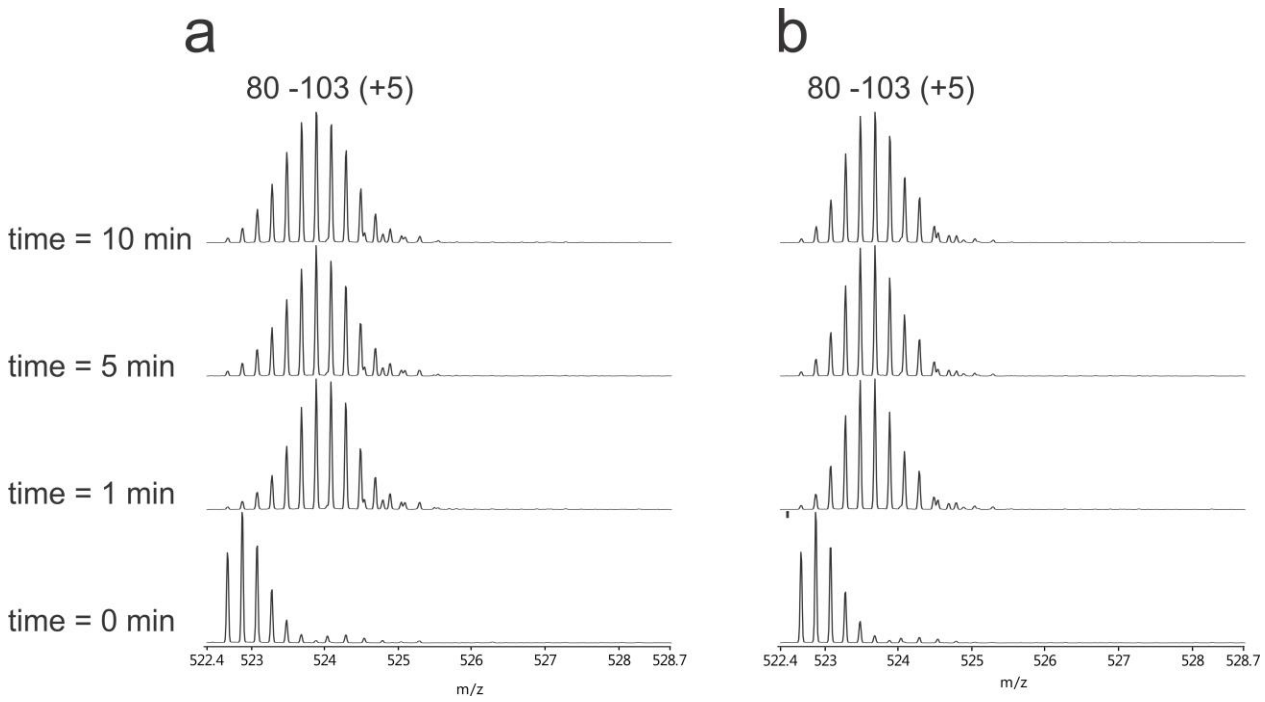

Figure S12. Mass spectra of +5 charge state ions of peptic peptide 80-103 obtained from (a) free and (b) ligand-bound CTB_5 at deuterium exposure times of 0, 1, 5 and 10 min.

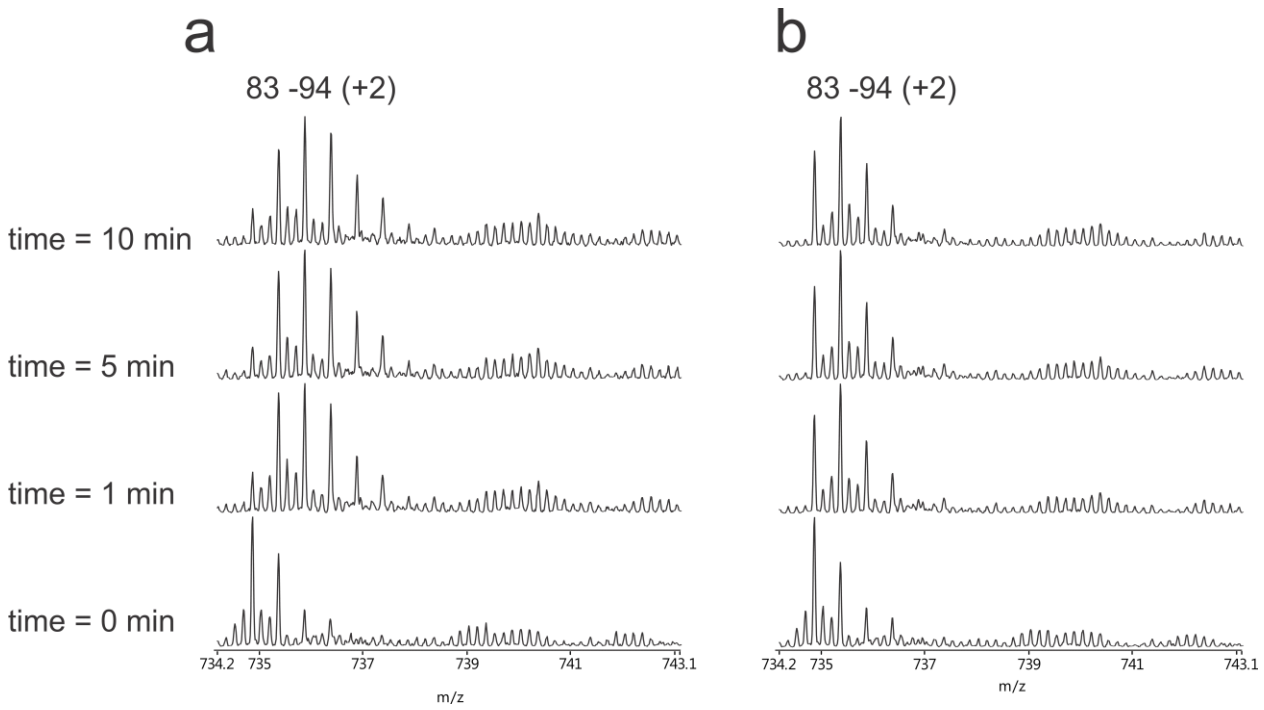

Figure S13. Mass spectra of doubly charged ions of peptic peptide 83-94 obtained from (a) free and (b) ligand-bound CTB_5 at deuterium exposure times of 0, 1, 5 and 10 min.

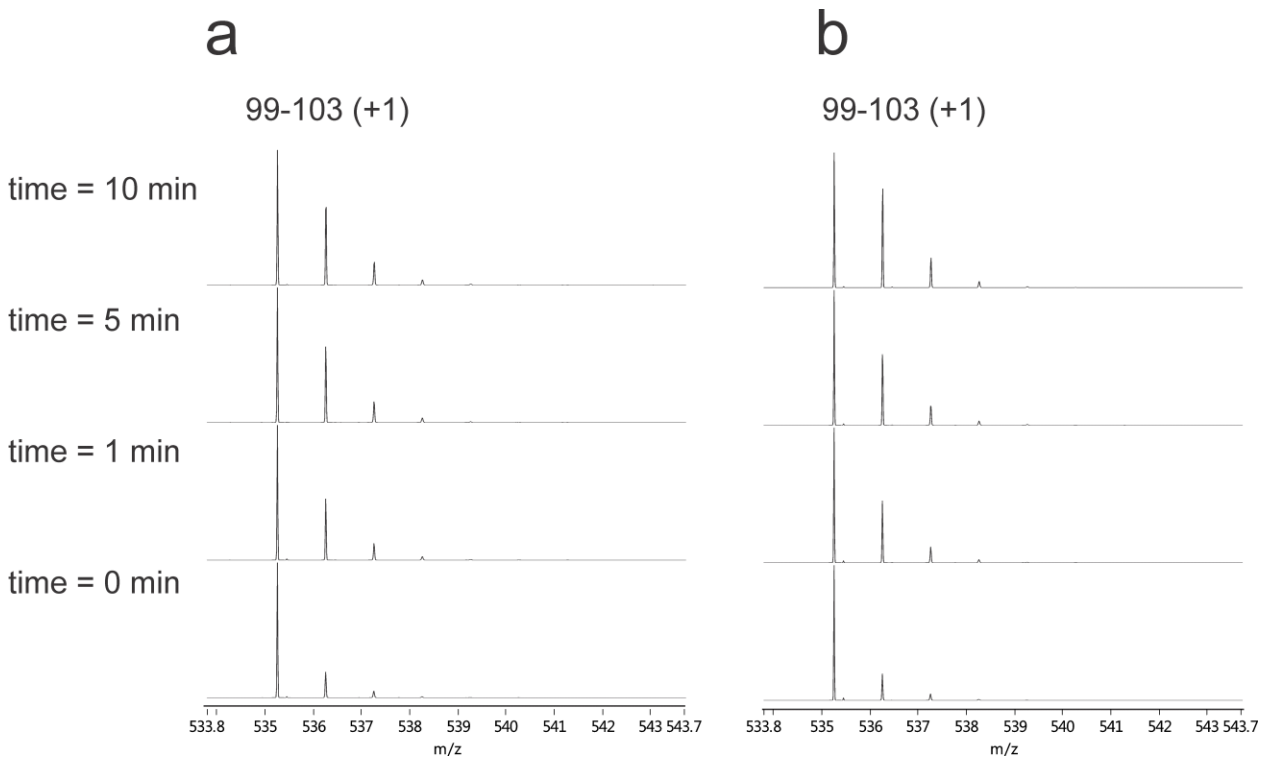

Figure S14. Mass spectra of singly charged ions of peptic peptide 99-103 obtained from (a) free and (b) ligand-bound CTB_5 at deuterium exposure times of 0, 1, 5 and 10 min.

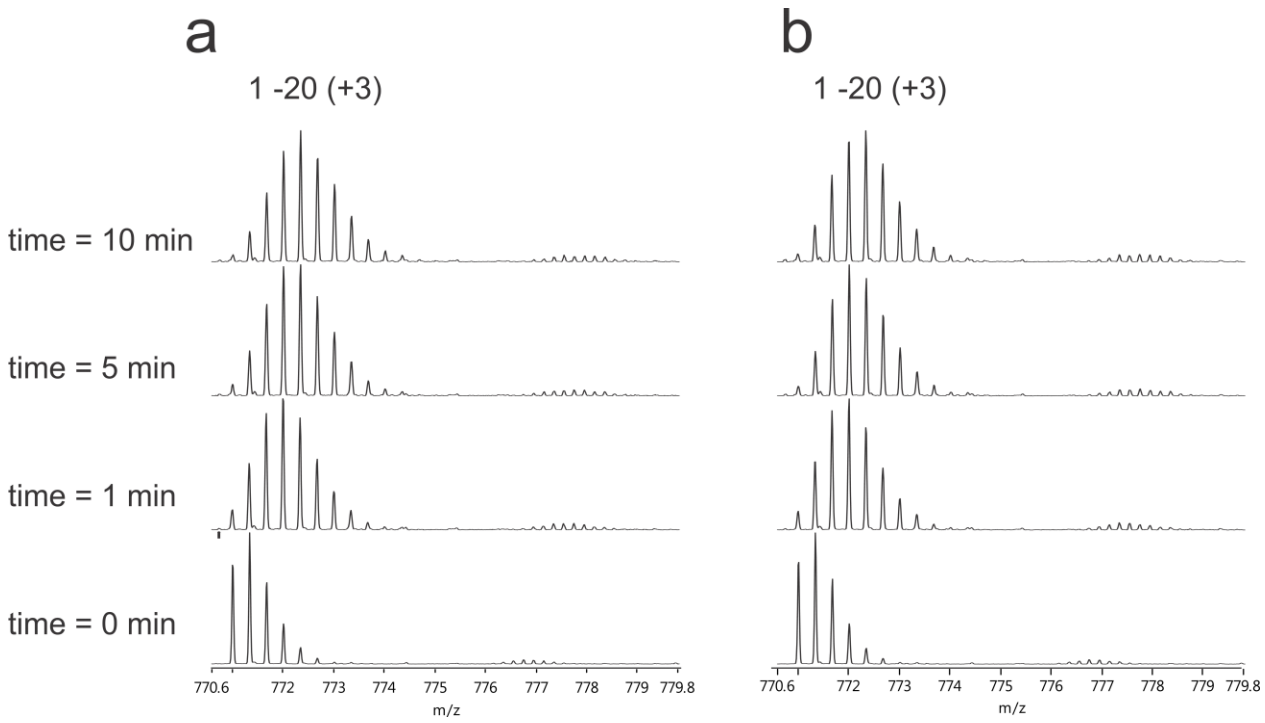

Figure S15. Mass spectra of triply charged ions of peptic peptide 1-20 obtained from (a) free and (b) ligand-bound $Stx1B_5$ at deuterium exposure times of 0, 1, 5 and 10 min.

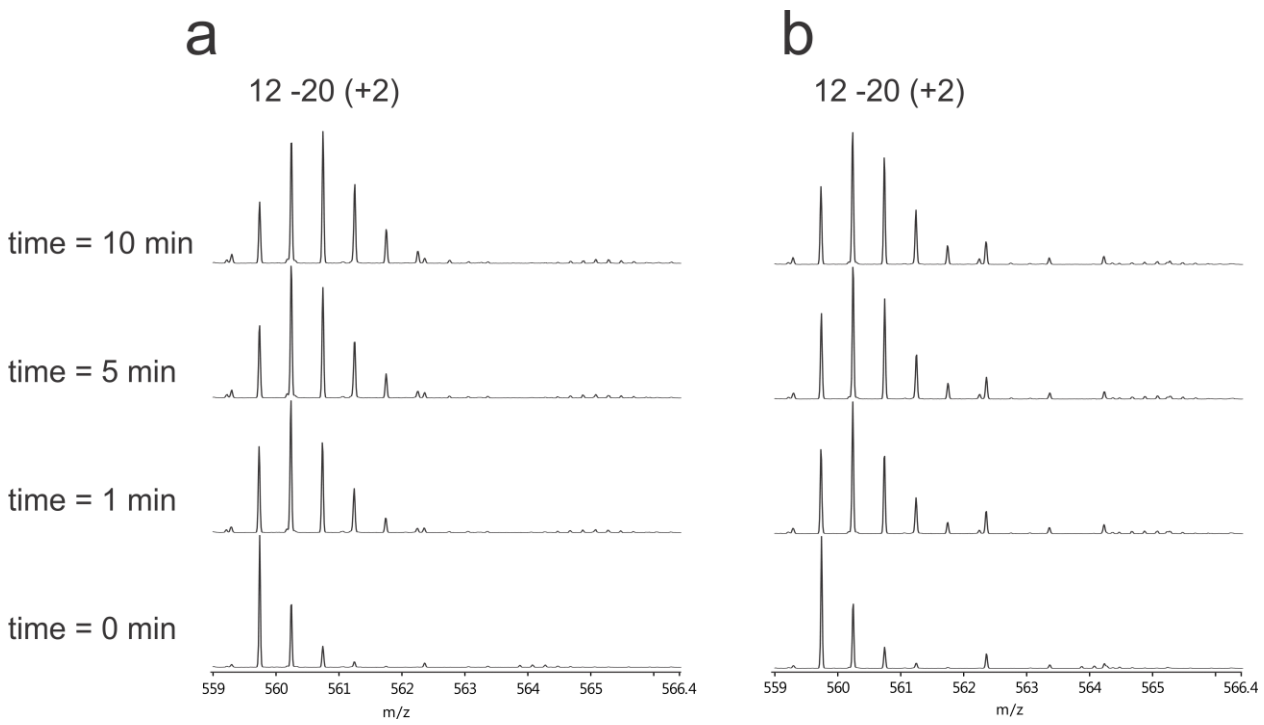

Figure S16. Mass spectra of doubly charged ions of peptic peptide 12-20 obtained from (a) free and (b) ligand-bound $Stx1B_5$ at deuterium exposure times of 0, 1, 5 and 10 min.

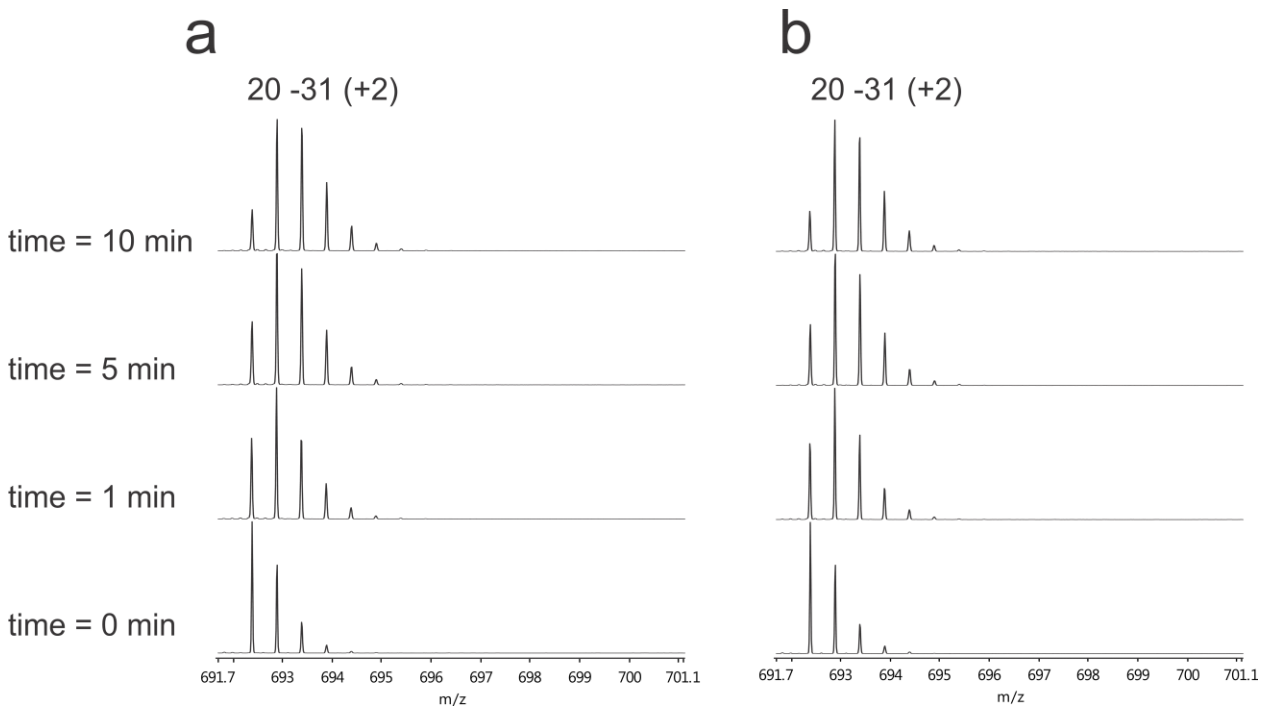

Figure S17. Mass spectra of doubly charged ions of peptic peptide 20-31 obtained from (a) free and (b) ligand-bound $Stx1B_5$ at deuterium exposure times of 0, 1, 5 and 10 min.

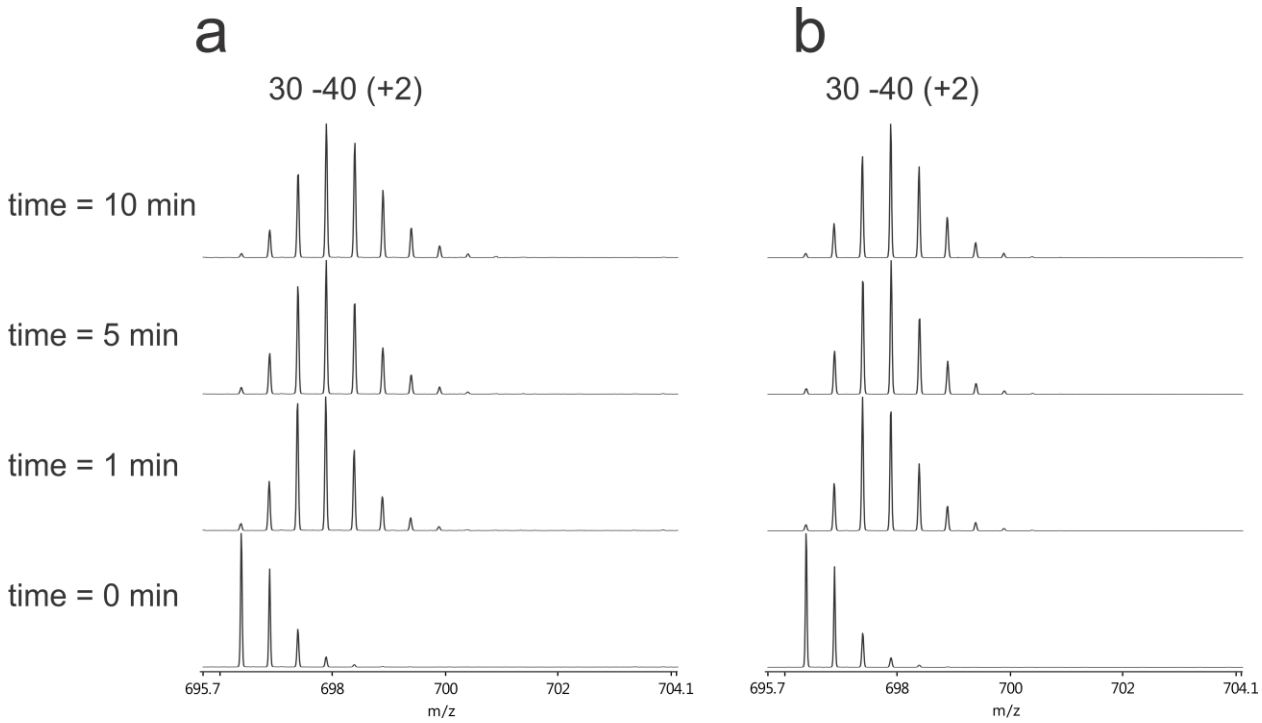

Figure S18. Mass spectra of doubly charged ions of peptic peptide 30-40 obtained from (a) free and (b) ligand-bound $Stx1B_5$ at deuterium exposure times of 0, 1, 5 and 10 min.

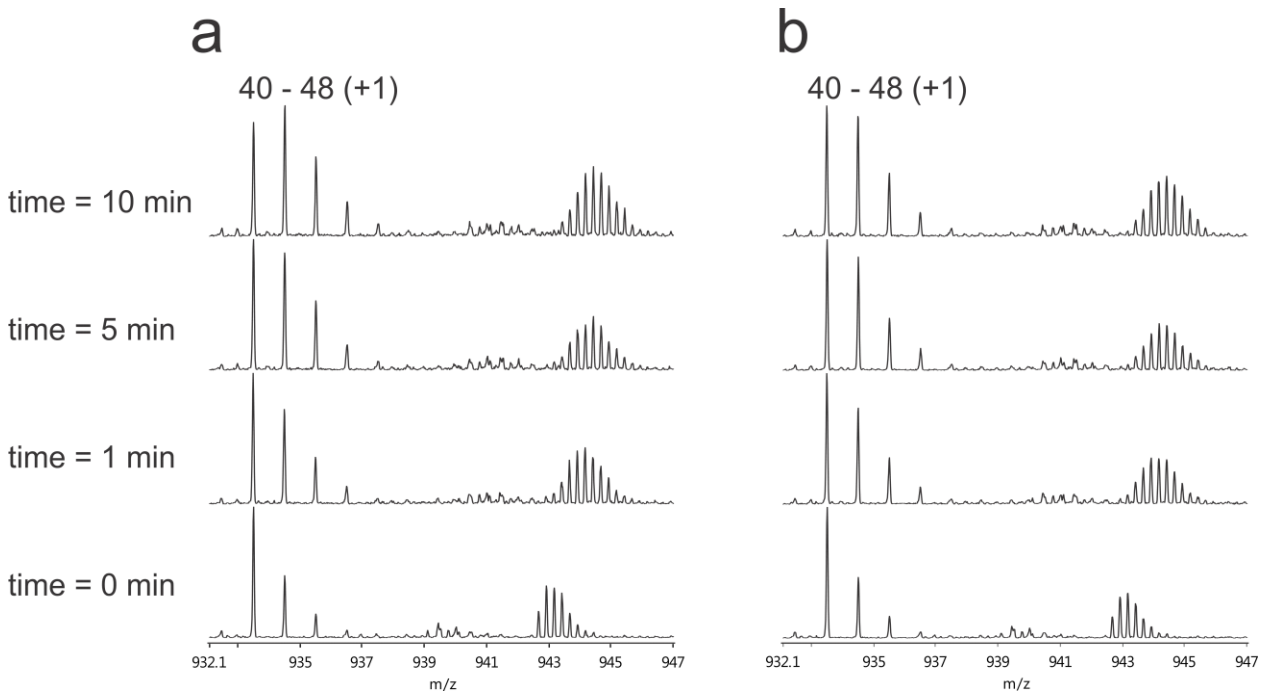

Figure S19. Mass spectra of singly charged ions of peptic peptide 40-48 obtained from (a) free and (b) ligand-bound $Stx1B_5$ at deuterium exposure times of 0, 1, 5 and 10 min.

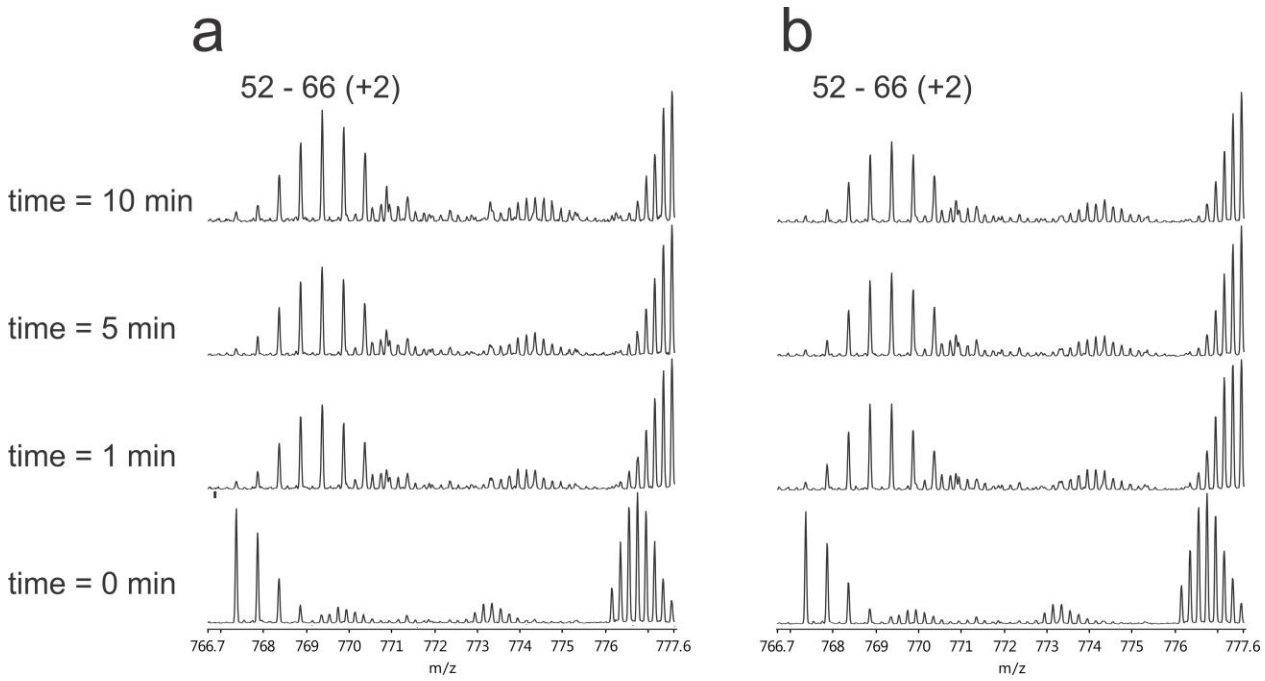

Figure S20. Mass spectra of doubly charged ions of peptic peptide 52-66 obtained from (a) free and (b) ligand-bound $Stx1B_5$ at deuterium exposure times of 0, 1, 5 and 10 min.

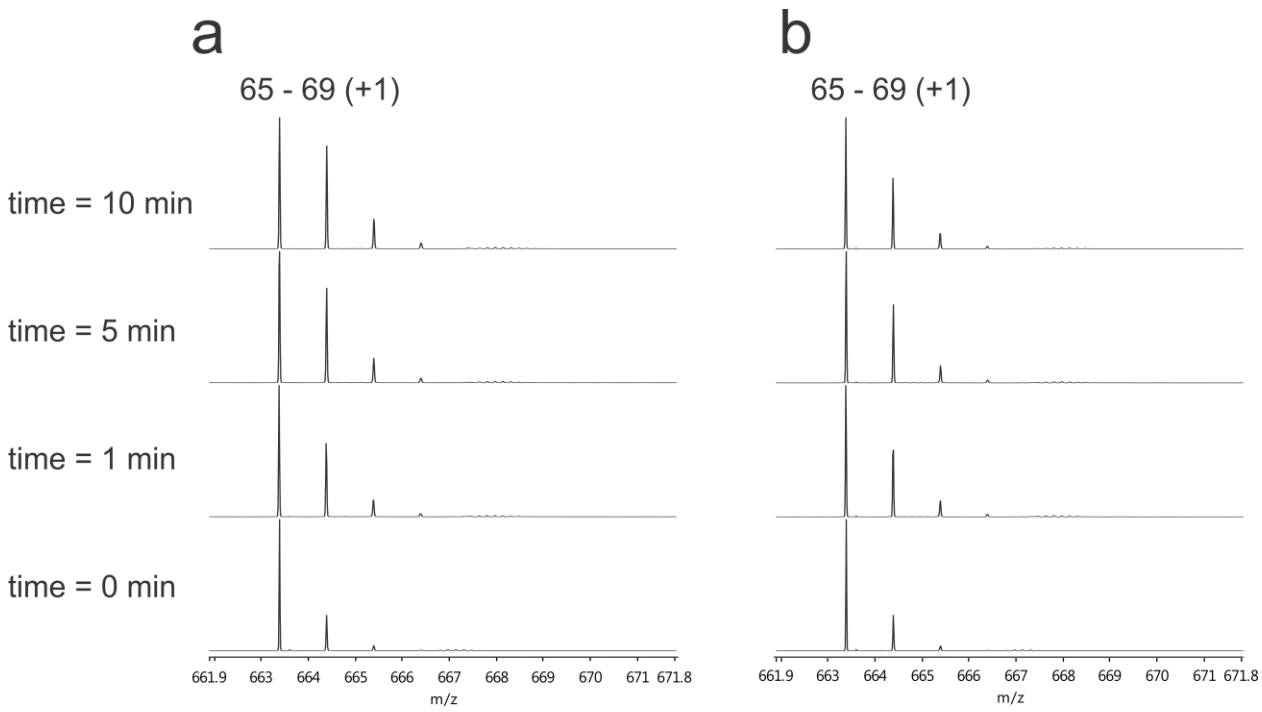

Figure S21. Mass spectra of singly charged ions of peptic peptide 65-69 obtained from (a) free and (b) ligand-bound $Stx1B_5$ at deuterium exposure times of 0, 1, 5 and 10 min.

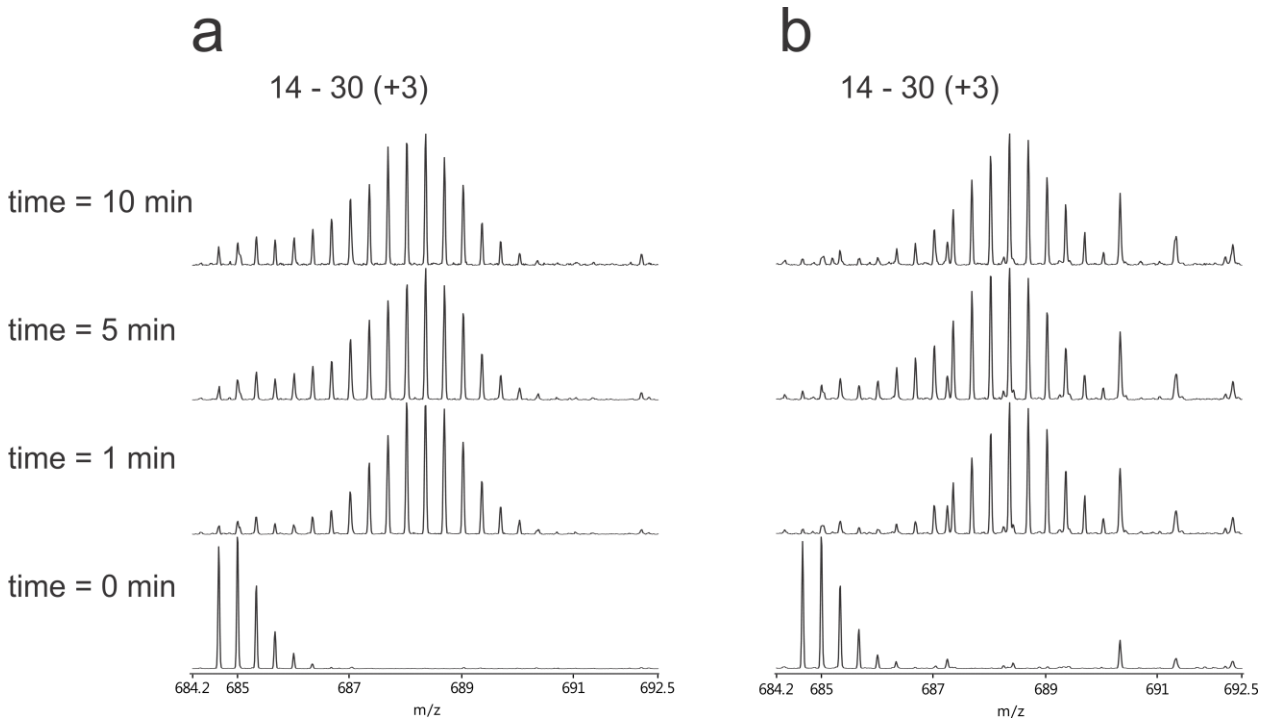

Figure S22. Mass spectra of triply charged ions of peptic peptide 14-30 obtained from (a) free and (b) ligand-bound TcdA-A2 at deuterium exposure times of 0, 1, 5 and 10 min.

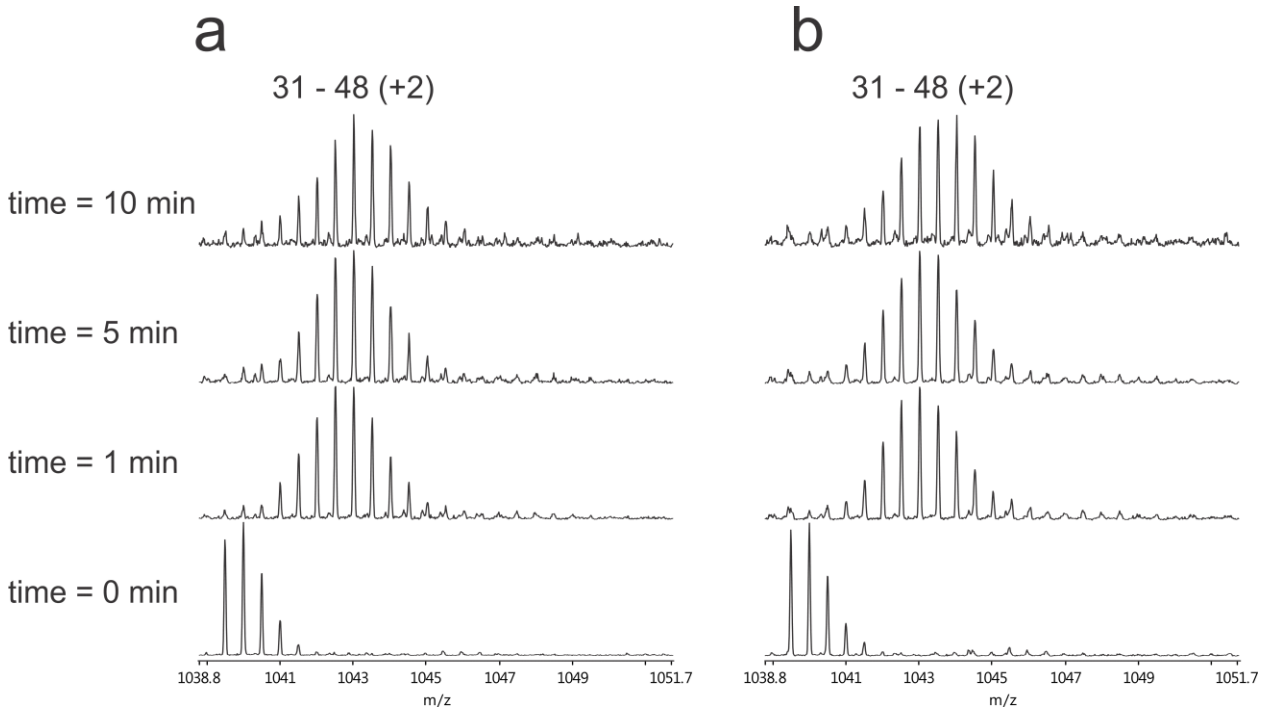

Figure S23. Mass spectra of doubly charged ions of peptic peptide 31-48 obtained from (a) free and (b) ligand-bound TcdA-A2 at deuterium exposure times of 0, 1, 5 and 10 min.

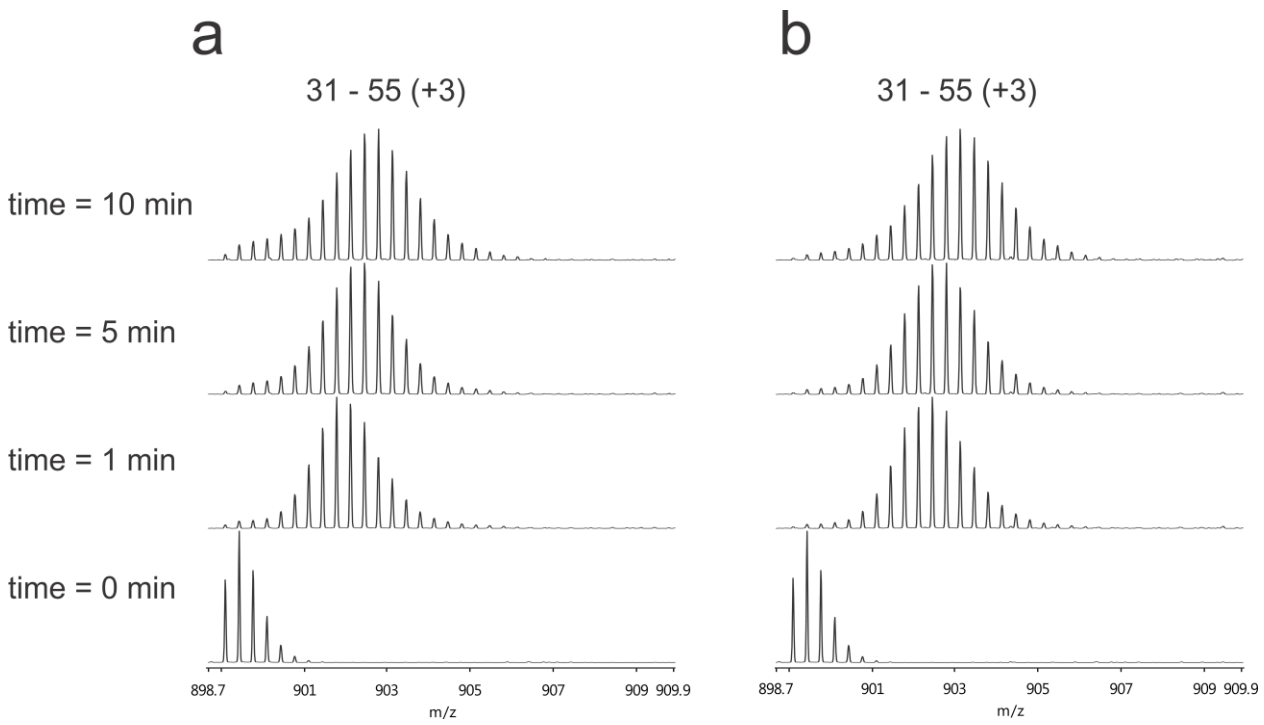

Figure S24. Mass spectra of triply charged ions of peptic peptide 31-55 obtained from (a) free and (b) ligand-bound TcdA-A2 at deuterium exposure times of 0, 1, 5 and 10 min.

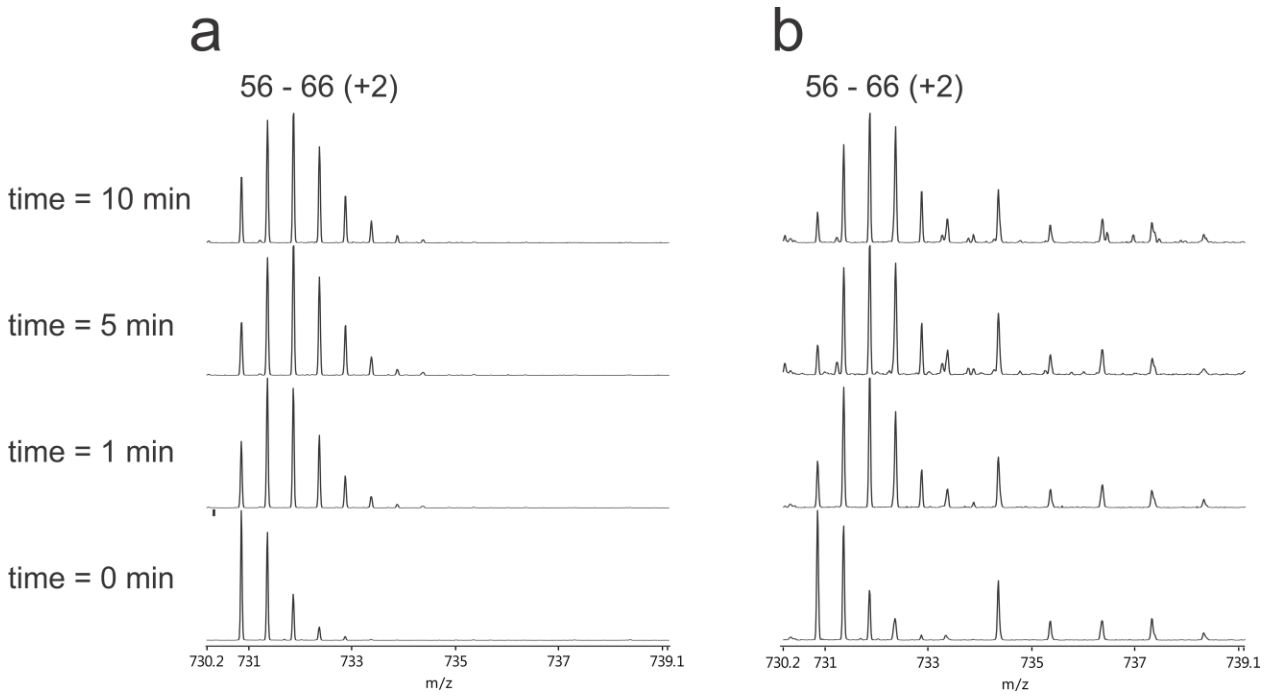

Figure S25. Mass spectra of doubly charged ions of peptic peptide 56-66 obtained from (a) free and (b) ligand-bound TcdA-A2 at deuterium exposure times of 0, 1, 5 and 10 min.

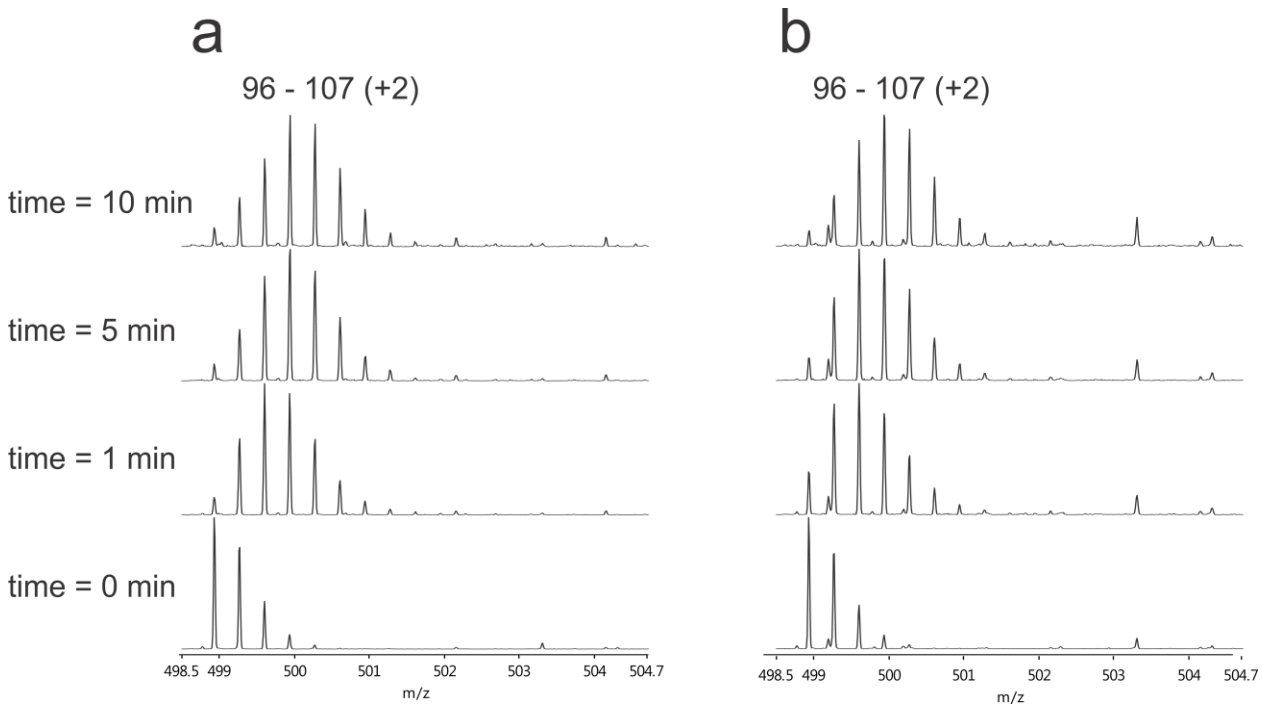

Figure S26. Mass spectra of doubly charged ions of peptic peptide 96-107 obtained from (a) free and (b) ligand-bound TcdA-A2 at deuterium exposure times of 0, 1, 5 and 10 min.

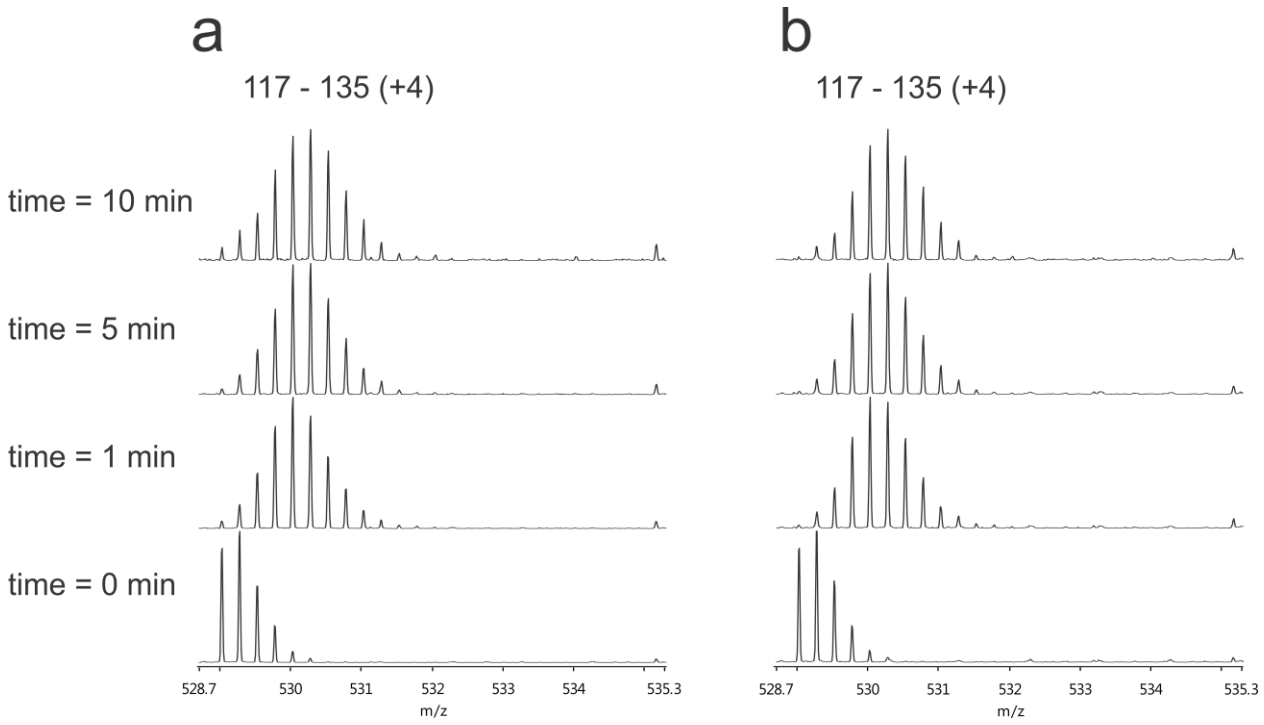

Figure S27. Mass spectra of quadruply charged ions of peptic peptide 117-135 obtained from (a) free and (b) ligand-bound TcdA-A2 at deuterium exposure times of 0, 1, 5 and 10 min.

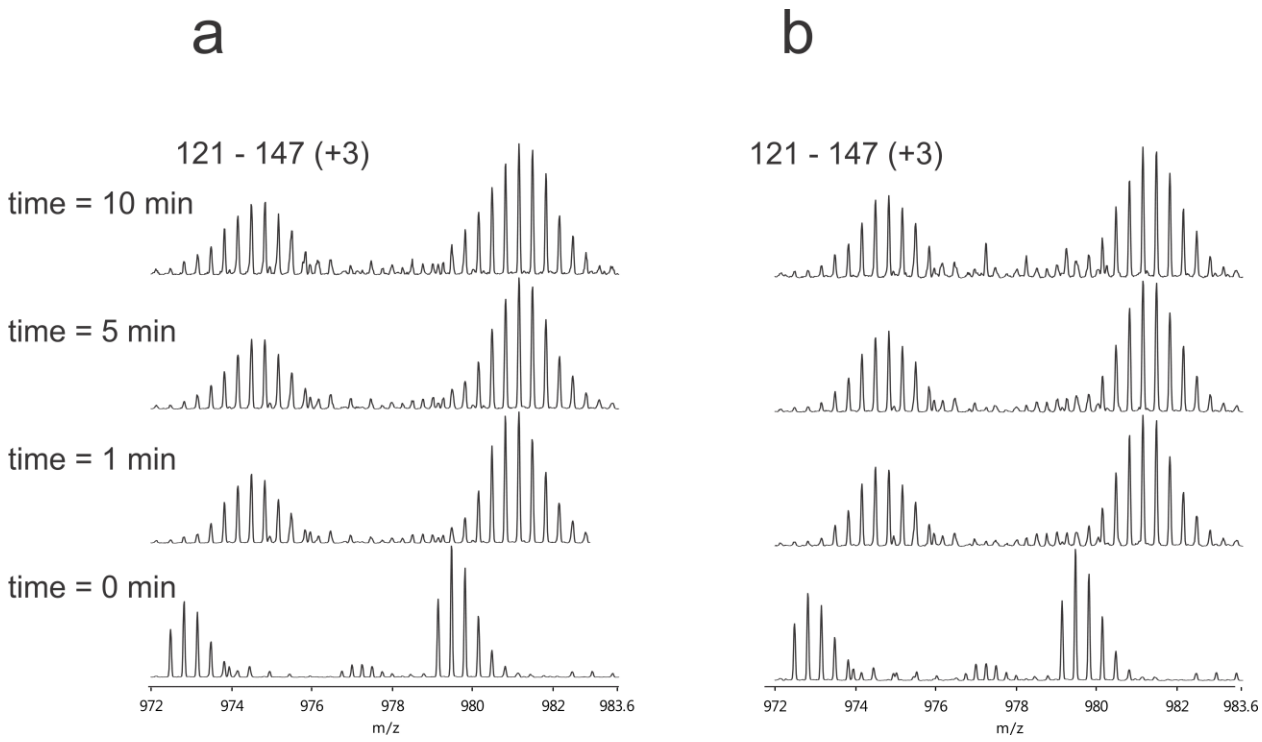

Figure S28. Mass spectra of triply charged ions of peptic peptide 121-147 obtained from (a) free and (b) ligand-bound TcdA-A2 at deuterium exposure times of 0, 1, 5 and 10 min.

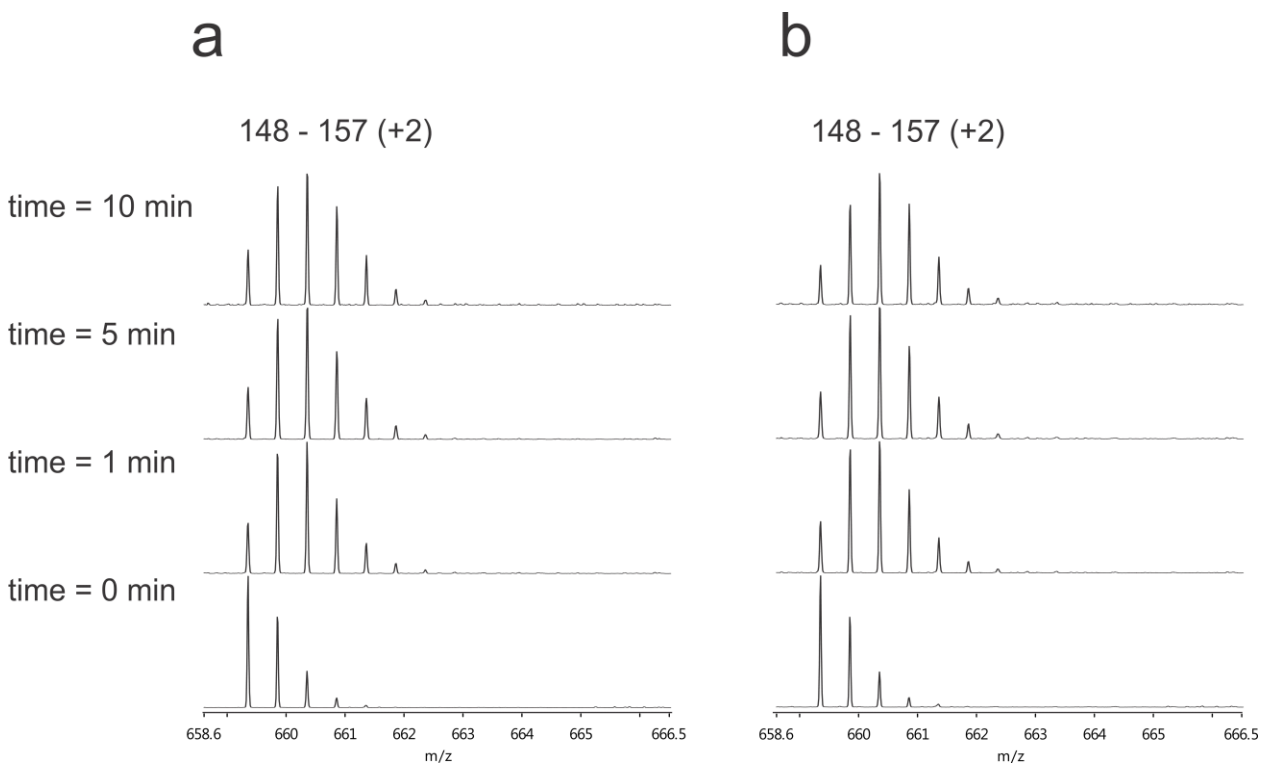

Figure S29. Mass spectra of doubly charged ions of peptic peptide 148-157 obtained from (a) free and (b) ligand-bound TcdA-A2 at deuterium exposure times of 0, 1, 5 and 10 min.

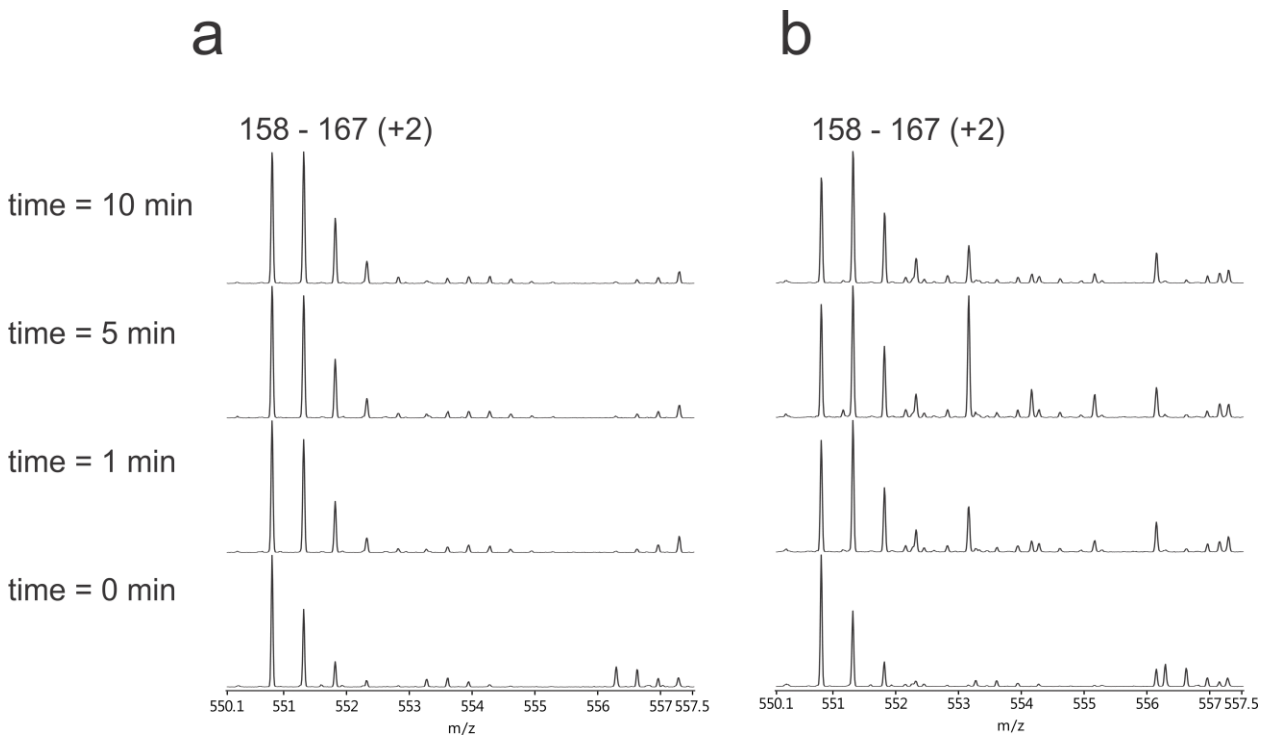

Figure S30. Mass spectra of doubly charged ions of peptic peptide 158-167 obtained from (a) free and (b) ligand-bound TcdA-A2 at deuterium exposure times of 0, 1, 5 and 10 min.

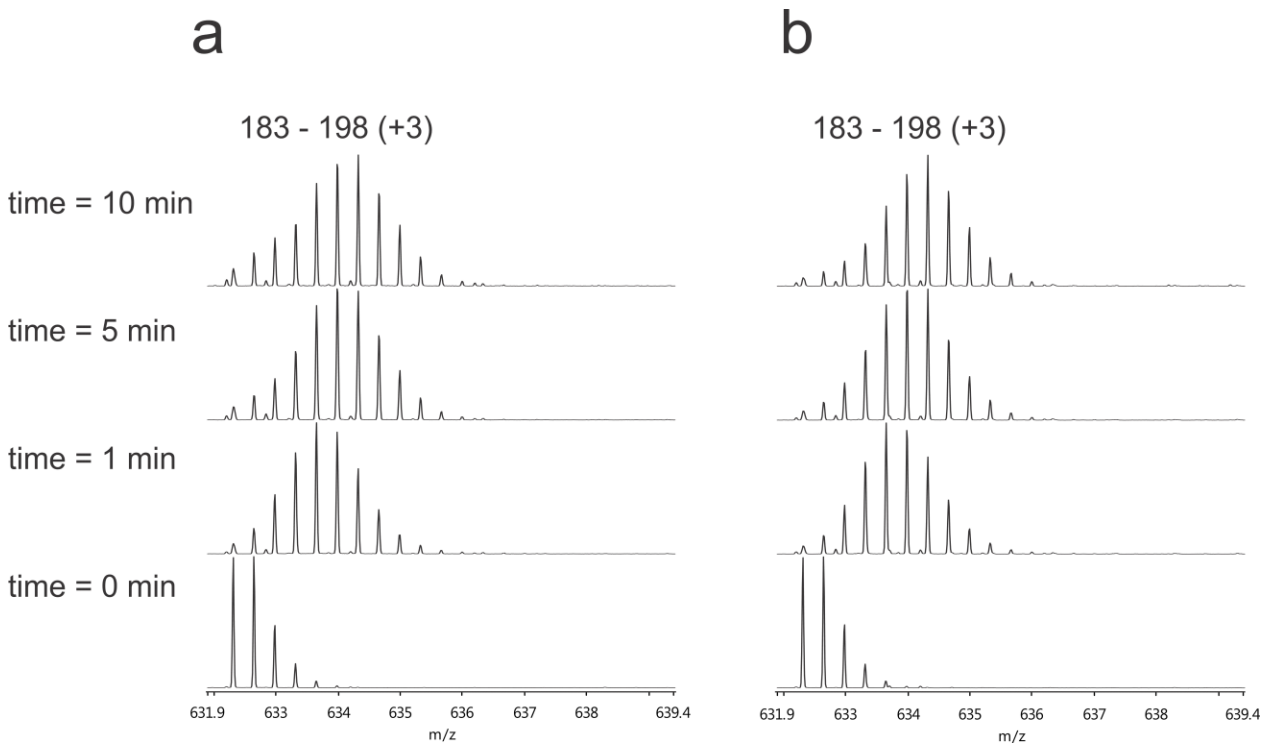

Figure S31. Mass spectra of triply charged ions of peptic peptide 183-198 obtained from (a) free and (b) ligand-bound TcdA-A2 at deuterium exposure times of 0, 1, 5 and 10 min.

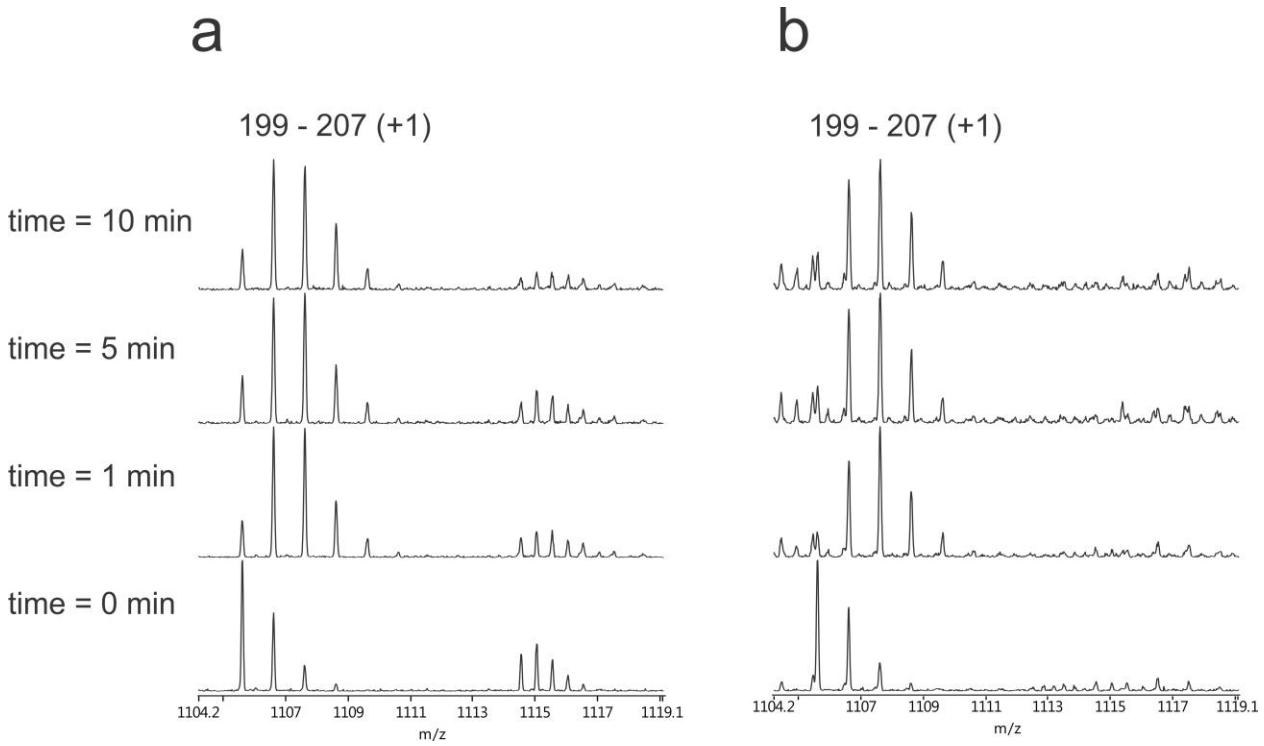

Figure S32. Mass spectra of singly charged ions of peptic peptide 199-207 obtained from (a) free and (b) ligand-bound TcdA-A2 at deuterium exposure times of 0, 1, 5 and 10 min.

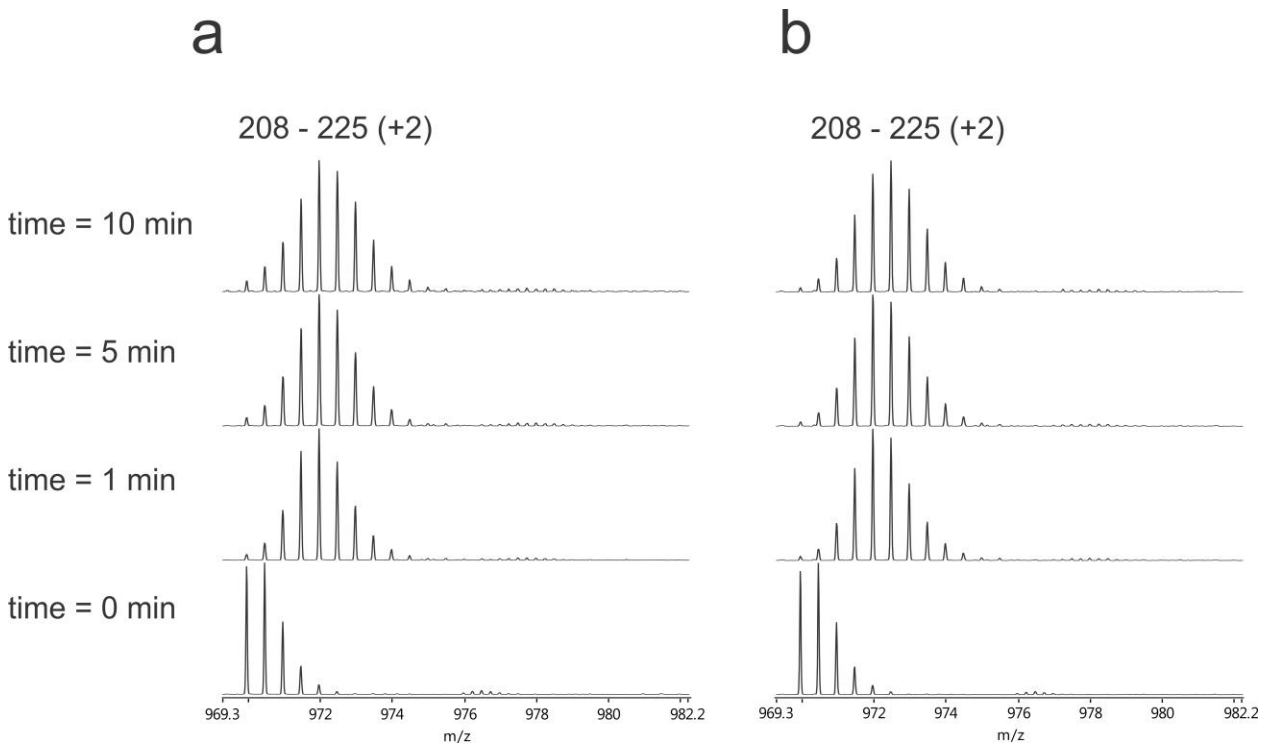

Figure S33. Mass spectra of doubly charged ions of peptic peptide 208-2250 obtained from (a) free and (b) ligand-bound TcdA-A2 at deuterium exposure times of 0, 1, 5 and 10 min.

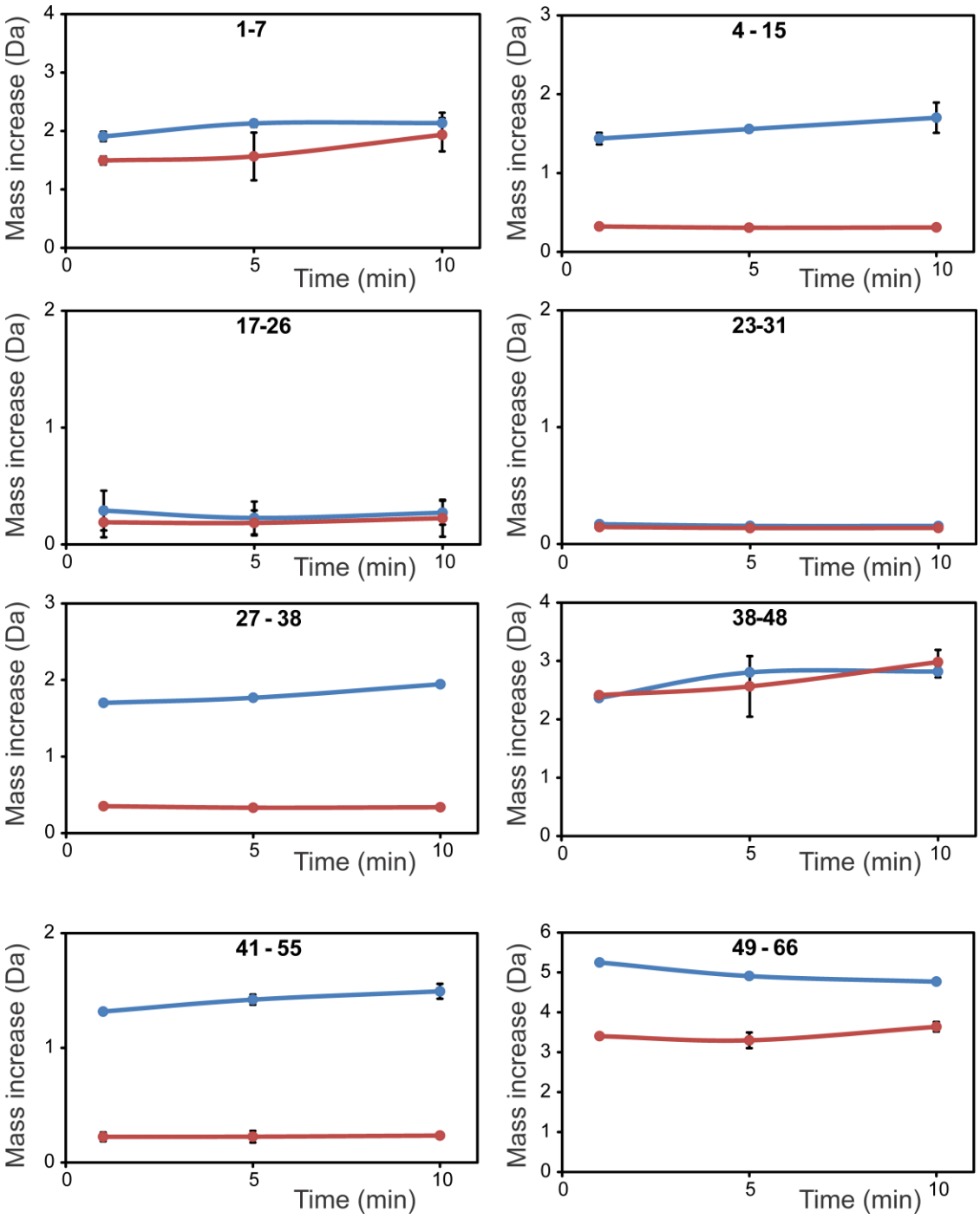
1-7
4 - 15
17-26
23-31
27 - 38
38-48
41 - 55
49 - 66
Mass increase (Da)
Time (min)

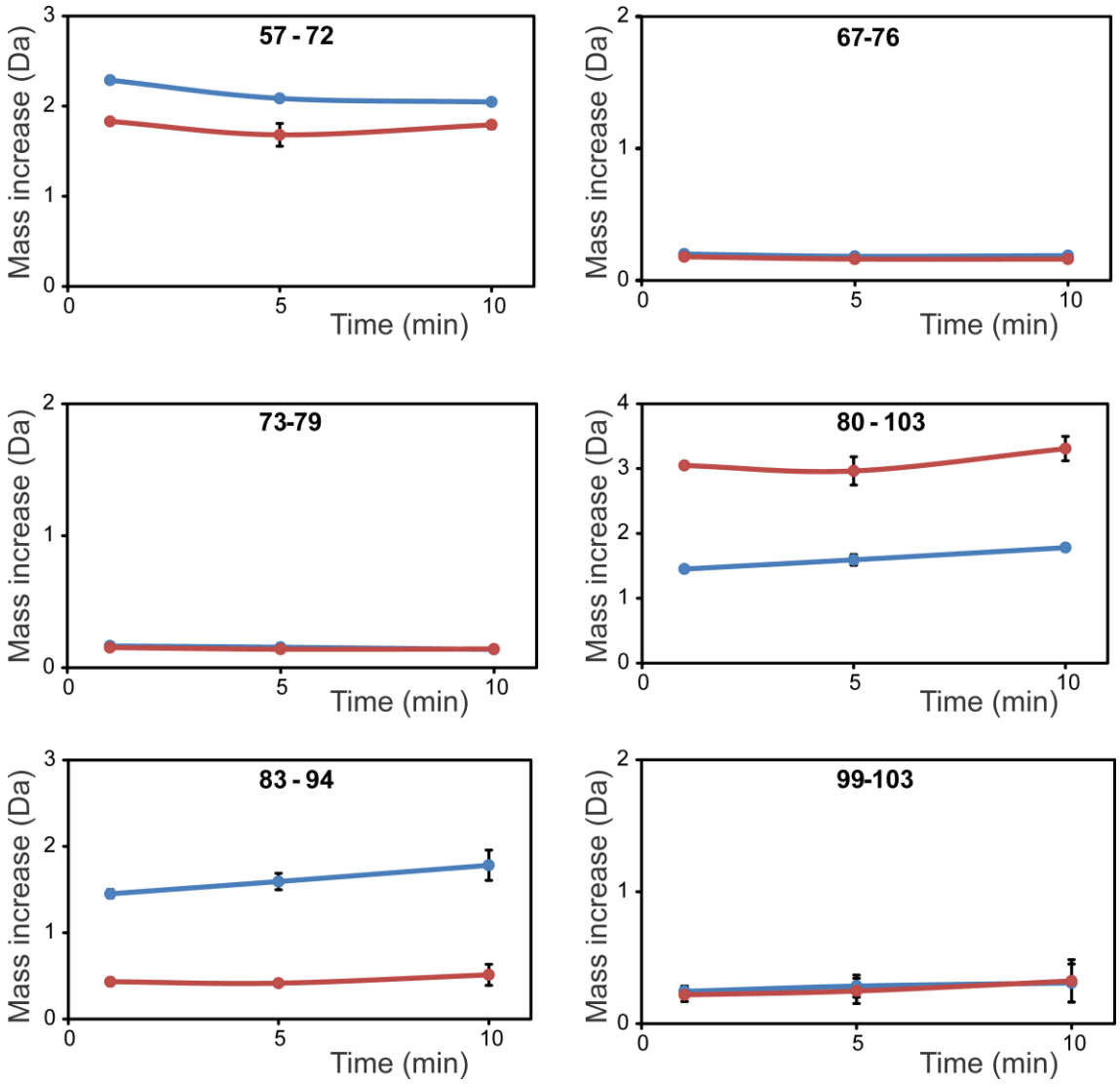

Figure S34. HDX kinetics measured for peptides produced from CTB_5 (blue) and (CTB_5 + 5GM1-os) (red).

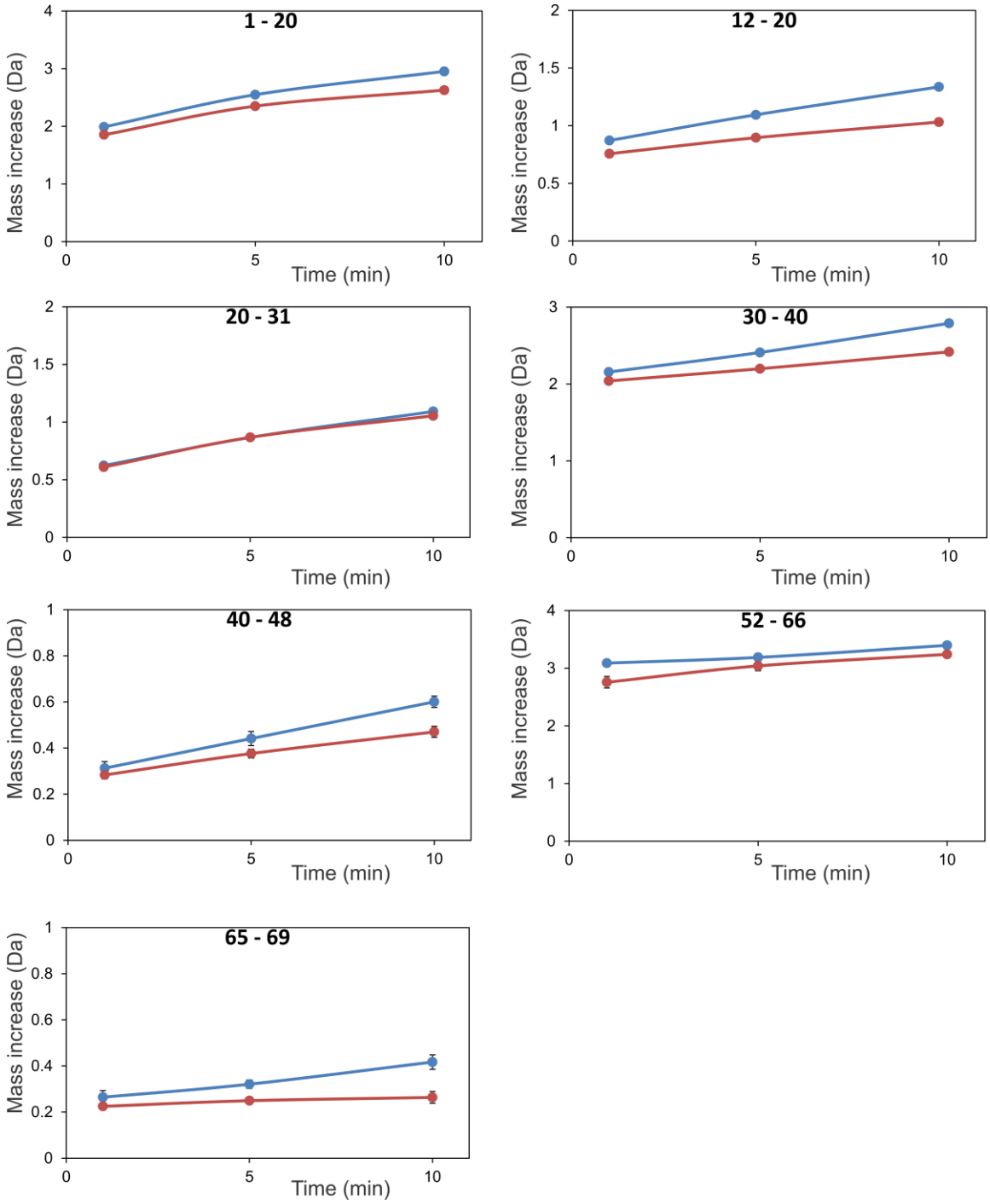

Figure S35. HDX kinetics measured for peptides produced from $Stx1B_5$ (blue) and ($Stx1B_5$ + 15Pk) (red).

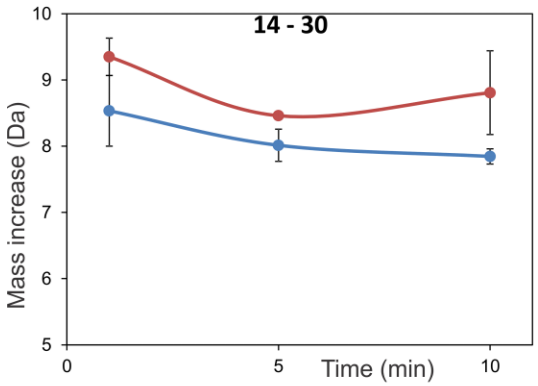
14 - 30
Mass increase (Da)
Time (min)

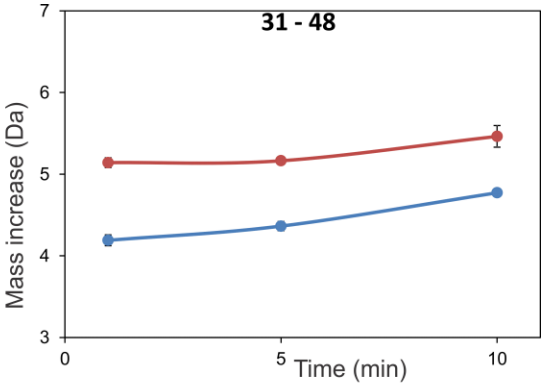
31 - 48
Mass increase (Da)
Time (min)

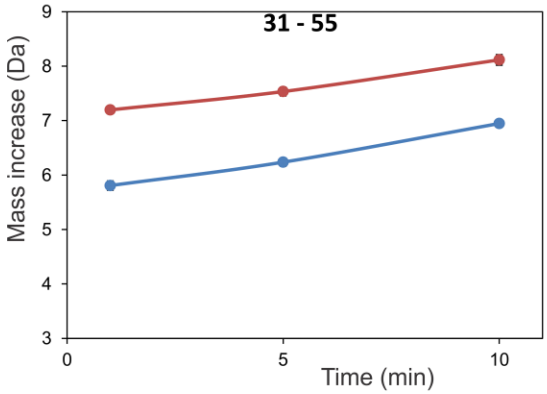
31 - 55
Mass increase (Da)
Time (min)

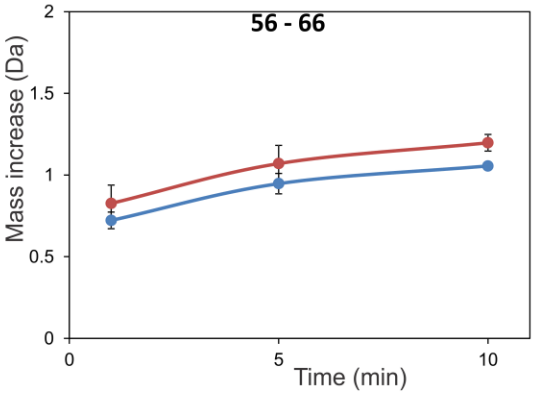
56 - 66
Mass increase (Da)
Time (min)

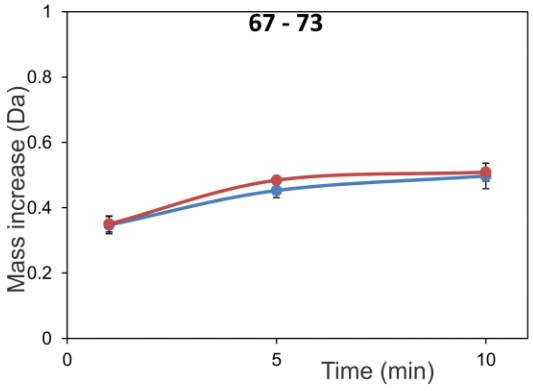
67 - 73
Mass increase (Da)
Time (min)

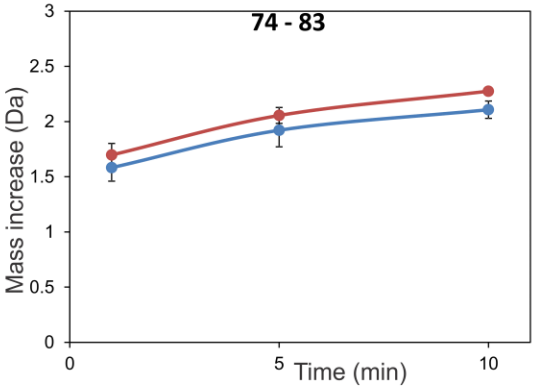
74 - 83
Mass increase (Da)
Time (min)

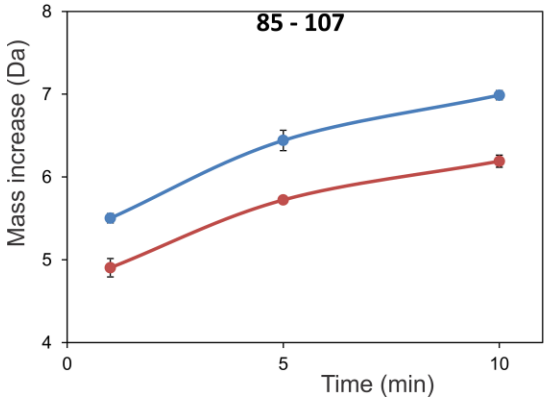
85 - 107
Mass increase (Da)
Time (min)

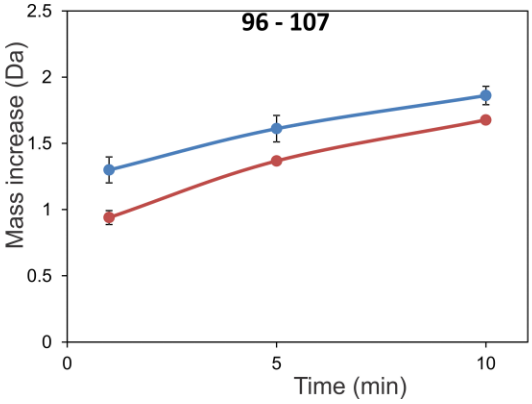
96 - 107
Mass increase (Da)
Time (min)

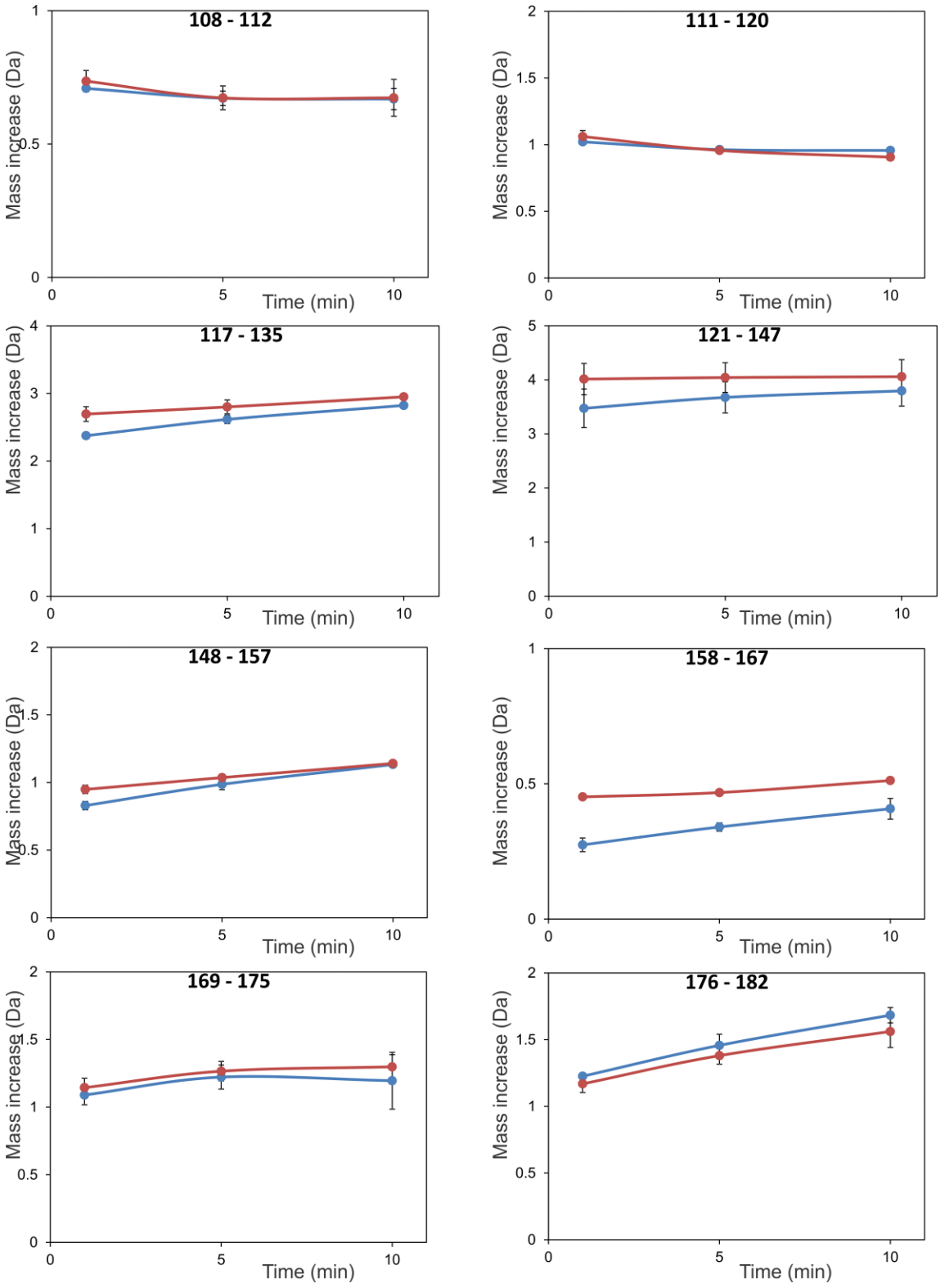
108 - 112
111 - 120
117 - 135
121 - 147
148 - 157
158 - 167
169 - 175
176 - 182
Mass increase (Da)
Time (min)

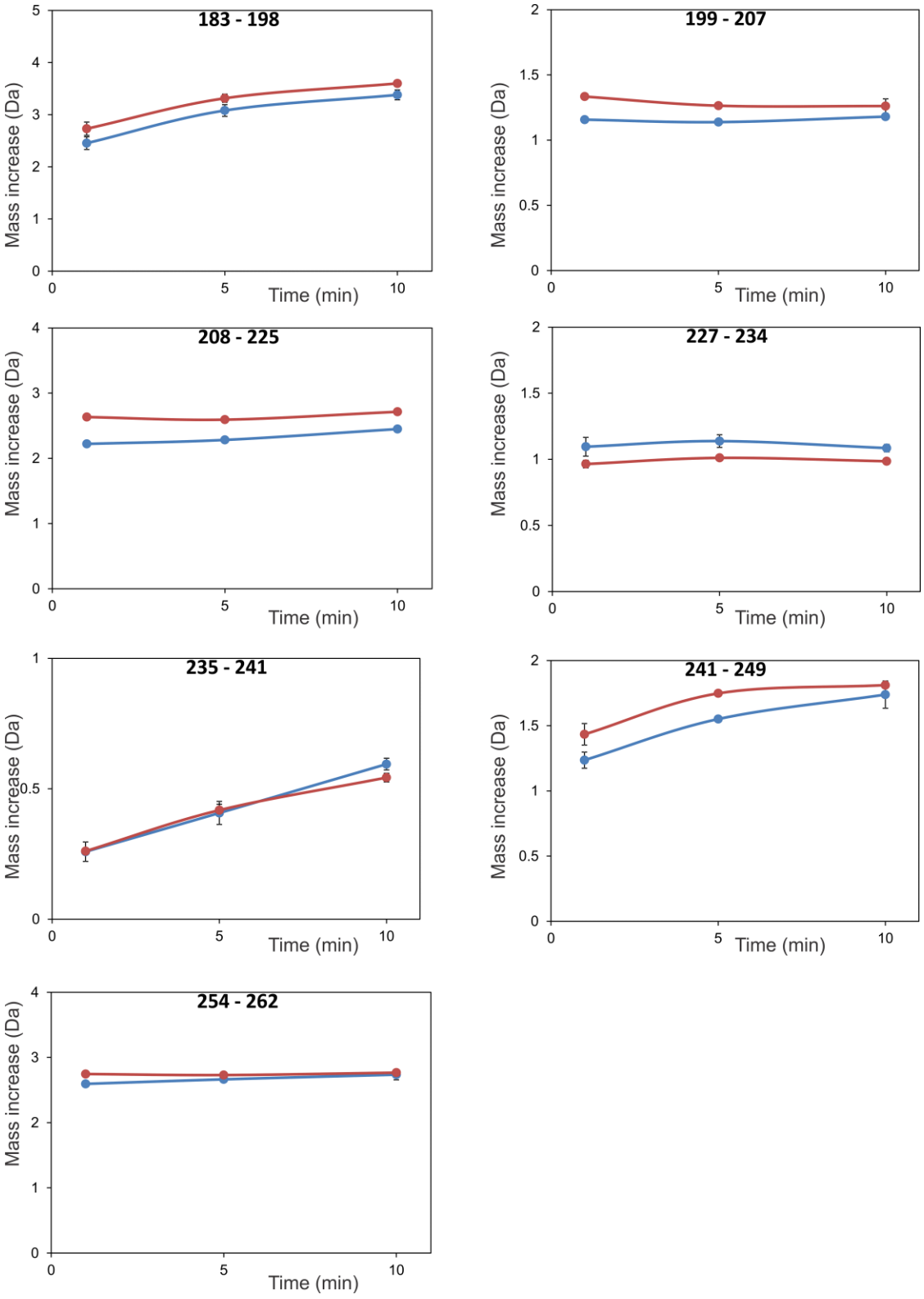

Figure S36. HDX kinetics measured for peptides produced from TcdA-A2 (blue) and (TcdA-A2 + 2CD-grease) (red).

Table S1. Results of Student's t-tests of ΔD_i values measured (at 1, 5 and 10 min) for free CTB_5 and the (CTB_5 + 5GM1-os) complex.

peptide	ΔD_i [a]	P value
1-7	1.2 ± 1.1	4×10^{-3}
4-15	3.8 ± 0.4	1×10^{-8}
17-26	0.2 ± 0.7	4×10^{-1}
23-31	0.1 ± 0.1	1×10^{-3}
27-38	4.4 ± 0.1	3×10^{-10}
38-48	0.0 ± 1.1	9×10^{-1}
41-55	3.5 ± 0.2	3×10^{-7}
49-66	4.6 ± 0.5	7×10^{-7}
57-72	1.1 ± 0.3	1×10^{-5}
67-76	0.1 ± 0.1	6×10^{-4}
73-79	0.0 ± 0.1	3×10^{-1}
80-103	3.9 ± 0.6	4×10^{-6}
83-94	3.5 ± 0.5	4×10^{-8}
99-103	0.0 ± 0.5	2×10^{-1}

a. Absolute error calculated by propagation of errors from 6 individual measurements.

Table S2. Results of Student's t-tests of ΔD_i values measured (at 1, 5 and 10 min) for free $Stx1B_5$ and the ($Stx1B_5$ + 15Pk) complex.

peptide	ΔD_i [a]	P value
1-20	0.7 ± 0.2	8×10^{-6}
12-20	0.6 ± 0.1	1×10^{-4}
20-31	0.1 ± 0.1	3×10^{-2}
30-40	0.7 ± 0.1	2×10^{-4}
40-48	0.2 ± 0.1	2×10^{-3}
52-66	0.6 ± 0.3	2×10^{-4}
65-69	0.3 ± 0.1	1×10^{-3}

a. Absolute error calculated by propagation of errors from 6 individual measurements.

Table S3. Results of Student's t-tests of ΔD_i values measured (at 1, 5 and 10 min) for free TcdA-A2 and (TcdA-A2 + 2CD-grease) complex.

peptide	ΔD_i [a]	P value
14-30	-2.2 ± 1.8	0.004
31-48	-2.4 ± 0.3	0.00002
31-55	-3.9 ± 0.3	0.000003
56-66	-0.4 ± 0.4	0.001
67-73	0.0 ± 0.1	0.056
74-83	-0.4 ± 0.5	0.001
85-107	2.1 ± 0.4	0.00003
96-107	0.8 ± 0.3	0.001
108-112	0.0 ± 0.2	0.25
111-120	0.0 ± 0.1	0.77
117-135	-0.6 ± 0.3	0.003
121-147	-1.2 ± 1.4	0.001
148-157	-0.2 ± 0.1	0.046
158-167	-0.4 ± 0.1	0.0004
169-175	-0.2 ± 0.5	0.020
176-182	0.3 ± 0.4	0.001
183-198	-0.7 ± 0.5	0.00001
199-207	-0.4 ± 0.1	0.001
208-225	-1.0 ± 0.1	0.00009
227-234	0.4 ± 0.2	0.00001
235-241	0.0 ± 0.1	0.54
241-249	-0.5 ± 0.3	0.01
254-262	-0.2 ± 0.2	0.03

a. Absolute error calculated by propagation of errors from 6 individual measurements.